nature biotechnology

Article

https://doi.org/10.1038/s41587-023-01900-x

Generation of precision preclinical cancer models using regulated in vivo base editing

Received: 14 July 2022

Accepted: 10 July 2023

Published online: 10 August 2023

Check for updates

Alyna Katti[1,2,11], Adrián Vega-Pérez[1,11], Miguel Foronda[1,7], Jill Zimmerman[1,2], Maria Paz Zafra[1,8], Elizabeth Granowsky[1], Sukanya Goswami[1], Eric E. Gardner[1], Bianca J. Diaz[1,2], Janelle M. Simon[3], Alexandra Wuest[3], Wei Luan[3], Maria Teresa Calvo Fernandez[1], Anastasia P. Kadina[4], John A. Walker II[4], Kevin Holden[4], Scott W. Lowe[3,5], Francisco J. Sánchez Rivera[3,9,10] & Lukas E. Dow[1,2,6]

Although single-nucleotide variants (SNVs) make up the majority of cancer-associated genetic changes and have been comprehensively catalogued, little is known about their impact on tumor initiation and progression. To enable the functional interrogation of cancer-associated SNVs, we developed a mouse system for temporal and regulatable in vivo base editing. The inducible base editing (iBE) mouse carries a single expression-optimized cytosine base editor transgene under the control of a tetracycline response element and enables robust, doxycycline-dependent expression across a broad range of tissues in vivo. Combined with plasmid-based or synthetic guide RNAs, iBE drives efficient engineering of individual or multiple SNVs in intestinal, lung and pancreatic organoids. Temporal regulation of base editor activity allows controlled sequential genome editing ex vivo and in vivo, and delivery of sgRNAs directly to target tissues facilitates generation of in situ preclinical cancer models.

Missense and nonsense mutations represent the vast majority of disease-associated genetic changes[1,2]. Cancer cells often harbor thousands of single base pair substitutions[3], and understanding the impact of specific variants is critical for defining disease drivers and highlighting therapeutic vulnerabilities. Although many model systems rely on gene 'knockout' or overexpression studies to interrogate the role of specific genes in disease states, ample evidence suggests that individual single-nucleotide variants (SNVs), even within the same gene[4–7] or codon[8], can dictate unique cancer phenotypes and response to targeted therapies.

Mice and organoids are powerful preclinical model systems, yet engineering cancer-associated SNVs in these complex settings is still laborious and inefficient. Cytosine and adenine base editing (BE) offer the most efficient approach to create targeted (C:G to T:A or A:T to G:C) SNVs[9–12]; however, efficient in vivo BE requires robust expression of editing enzymes that is limited by adequate delivery and can induce antigen-driven immune responses[8,13–20]. Improving the ease, efficiency and control with which base editors and SNVs can be generated in complex cell systems will streamline the functional annotation of disease-associated genetic changes.

Here we describe a mouse model carrying an expression-optimized, inducible and regulated cytosine base editor (BE3RA[8]) to enable temporal control of BE in a wide variety of murine tissues. We show that transient expression of a single inducible base editing (iBE) enzyme is

[1]Sandra and Edward Meyer Cancer Center, Weill Cornell Medicine, New York, NY, USA. [2]Graduate School of Medical Sciences, Weill Cornell Medicine, New York, NY, USA. [3]Cancer Biology and Genetics, Memorial Sloan Kettering Cancer Center, New York, NY, USA. [4]Synthego Corporation, Redwood City, CA, USA. [5]Howard Hughes Medical Institute, Memorial Sloan Kettering Cancer Center, New York, NY, USA. [6]Department of Medicine, Weill Cornell Medicine, New York, NY, USA. [7]Present address: Memorial Sloan Kettering Cancer Center, New York, NY, USA. [8]Present address: Biosanitary Research Institute (IBS)–Granada, Granada, Spain. [9]Present address: David H. Koch Institute for Integrative Cancer Research, Massachusetts Institute of Technology, Cambridge, MA, USA. [10]Present address: Department of Biology, Massachusetts Institute of Technology, Cambridge, MA, USA. [11]These authors contributed equally: Alyna Katti, Adrián Vega-Pérez. e-mail: lud2005@med.cornell.edu

capable of driving highly efficient BE in pancreatic, lung and intestinal organoids. Furthermore, we demonstrate that iBE can be used in combination with somatic sgRNA delivery to build in vivo preclinical models of hepatocellular carcinoma (HCC) and pancreas ductal adenocarcinoma (PDAC) harboring single or multiple specific cancer-associated SNVs. In all, iBE is a unique tool for efficient modeling of SNVs in physiologically accurate preclinical models to define and test their impact in tumor initiation and progression.

Results

Tightly regulated in vivo expression of an optimized base editor

To derive mice carrying an iBE allele, we injected KH2 mouse embryonic stem cells (ESCs) harboring a single copy of an expression-optimized TRE-BE3RA transgene downstream of the *Col1a1* locus[8] (Fig. 1a and Extended Data Fig. 1a,b) into albino B6 blastocysts. High chimerism (agouti) founders were then backcrossed to C57Bl/6 mice for at least four generations before analysis. In the absence of doxycycline (dox), the iBE allele transmitted at normal Mendelian ratios and could be maintained as a heterozygous or homozygous colony (Supplementary Table 1 and Extended Data Fig. 1c). We previously showed that induction of dox-regulated transgenes at the *Col1a1* locus with a constitutively expressed third-generation reverse tet-transactivator (CAGs-rtTA3) allele drives uniform expression across a broad range of murine cell types, particularly epithelial tissues[21,22]. To evaluate expression in the iBE mouse, we generated CAGs-rtTA3$^{+/-}$;iBE$^{+/-}$ (iBE hemizygous or 'iBE^{hem}') mice and fed them dox chow (200 mg kg^{-1}) for 1 week. All tissues examined showed dox-dependent induction of BE3RA that could be reversed after dox withdrawal (dox switched, or 'SW') (Fig. 1b). No tissues showed evidence of BE protein expression in the absence of dox, although RNA sequencing (RNA-seq) of intestinal tissue revealed a low, but detectable, amount of BE3RA transcript (~1 per 1 M transcripts) (Fig. 1d). Unlike the uniform induction seen in GFP-shRNA transgenes at the *Col1a1* locus[21,22], BE3RA appeared heterogeneous across multiple tissues (Fig. 1c and Extended Data Fig. 1e). We reasoned this was likely due to stochastic silencing of either CAGs-rtTA3 or iBE transgenes during embryogenesis. To test this, we generated mice carrying one or two copies of each allele and examined expression across a range of tissues (Extended Data Fig. 2). The presence of two rtTA3 alleles (CAGs-rtTA3$^{+/+}$;iBE3$^{+/-}$) increased the uniformity of BE3RA expression, and this was further improved in mice carrying two iBE alleles (CAGs-rtTA3$^{+/-}$;iBE$^{+/+}$) (Extended Data Fig. 2). As expected, CAGs-rtTA3$^{+/+}$;iBE$^{+/+}$ ('iBE^{hom}') mice showed the most consistent and uniform expression of BE3RA across liver, pancreas, small intestine and colon (Fig. 1c,d and Extended Data Fig. 1e). Despite increased overall expression in iBE^{hom} animals, transcript and protein expression returned to baseline within 1 week of dox withdrawal (Fig. 1c,d). RNA-seq analysis revealed minimal change to cellular transcriptomes in the intestine and liver of iBE^{hom} mice, with no pattern of differential gene expression associated specifically with induction of the BE enzyme (Fig. 1e,f and Supplementary Table 2), with the largest expression change being the BE enzyme itself (Fig. 1e and Supplementary Table 2). Consistent with these data, no histological abnormalities or differences in immune cell populations were observed in iBE^{hom} animals treated with or without dox for 2 weeks (Extended Data Fig. 3a,b).

Minimal off-target RNA and DNA editing in iBE mice

Previous studies reported that BE enzymes can produce widespread, sgRNA-independent off-target RNA editing[23]. To determine if RNA editing could be a concern in iBE mice, we analyzed mRNA from the liver and intestine of iBE^{hom} mice (or CAGs-rtTA3-only controls) treated with or without dox for 2 weeks and those treated for 2 weeks and withdrawn from dox for 6 d. Analysis of transfected HEK293T cells from previously published data[23] showed a marked 280-fold increase in C > U edited RNA transcripts (1,880 C > U variants per 1 M reads) relative to control (~7 C > U variants per 1 M reads) (Extended Data Fig. 4a). Similarly, muscle tissue from recently published transposon-based BE3 transgenic mice[24] showed a 30-fold increase in C > U variants (~380 versus ~12 C > U variants per 1 M reads) (Extended Data Fig. 4a). In comparison, iBE^{hom} tissues showed much lower levels of C > U RNA editing in liver (~36 C > U variants per 1 M reads) and intestine (~19 variants per 1 M reads) in dox-treated samples, representing a six-fold and three-fold increase over controls, respectively. Furthermore, this moderate increase was almost entirely reversed within 6 d of withdrawing dox chow (Extended Data Fig. 4a). Non-C > U editing levels remained unchanged over all conditions (Extended Data Fig. 4b). One possible explanation for the difference in editing frequency between our model and previous reports is the relative level of BE enzyme expression between experimental systems. Indeed, BE3 transcript was ~70-fold higher in transfected HEK293T cells than dox-treated iBE tissues (Extended Data Fig. 4c).

In addition to RNA editing, we assessed the possibility of DNA off-target effects using iBE-targeted ESCs expressing *Apc*^{Q1405} and *Pik3ca*^{E545K} sgRNAs. Using ESCs enables the reliable growth and isolation of clonal populations after iBE induction by dox treatment to ensure that any infrequent mutations can be detected. In total, we assessed 60 dox-treated clones and 60 no-dox control clones (in pools of 10) using ultra-deep sequencing (800–1,000× coverage) of a focused panel of cancer-relevant genes (MSK-IMPACT[25]). We saw no evidence of increased C > T DNA editing in dox-treated cells relative to controls (Extended Data Fig. 5 and Supplementary Table 3).

Together, these data show that the iBE transgene can be induced and repressed uniformly across a range of murine tissues and that low levels of C > U RNA editing can be quickly reversed by withdrawal of transgene expression.

Efficient single and multiplexed editing in iBE organoids

Organotypic cell culture models or 'organoids' are a powerful systems to study epithelial biology. We and others have used organoids to reveal the contribution of cancer-associated nonsense and missense mutations for cell behavior and drug response[26,27]; however, efficient introduction of SNVs using BE is a substantial practical challenge in scaling up the generation of large collections of tailored model systems. To determine if cells derived from iBE mice could streamline

Fig. 1 | Regulatable BE expression across murine tissues. a, Schematic representation of iBE mice containing *R26-CAGs-rtTA3* allele and *TRE-BE3RA* allele. **b**, Cas9 immunoblot on bulk tissue, as indicated, from iBE^{hem} mice maintained on normal chow (day 0, −dox), dox chow for 7 d (day7, +dox) or dox switched from dox chow for 7 d to normal chow for 7 d (day 14, −dox) across tissues bulk harvested for protein. β-actin, loading control. Molecular weight: β-actin (42 kDa), BE3RA (160 kDa). Blots are representative of two independent experiments for each condition. **c**, Immunofluorescent detection of Cas9 protein in iBE^{hem} (top) or iBE^{hom} (bottom) mice maintained on normal chow (no dox) or dox chow for 7 d (day 7 dox) or dox switched from dox chow for 7 d to normal chow for 7 d (dox SW). Cas9 protein (green), DAPI staining for nuclei (blue) across four tissues analyzed. Data are representative of three independent mice for each condition (see Extended Data Fig. 1e for individual replicates). **d**, Transcript abundance (transcripts per million (TPM)) in intestine and liver from rtTA^{hem} and iBE^{hom} on normal chow (−), dox chow (+) for 14 d or switched from dox chow for 14 d to normal chow for 6 d (SW). Data are presented as mean values ± s.d., $n = 3$ mice per genotype/condition. **e**, Volcano plots from RNA-seq data comparing rtTA^{hem} versus iBE^{hom} maintained on dox chow for 14 d ($n = 3$ mice). **f**, Heat map of differentially expressed (DE) genes from intestine and liver from rtTA^{hem} and iBE^{hom} on normal chow (−), dox chow (+) for 14 d or switched from dox chow for 14 d to normal chow for 6 d (SW). Includes DE genes between all conditions within the intestine and liver groups; does not include DE genes between different tissues ($n = 3$ mice per genotype/condition). D, day; NS, not significant.

https://doi.org/10.1038/s41587-023-01900-x

the creation of targeted mutations ex vivo, we generated organoids from small intestine, pancreas and basal cells from the trachea of iBE mice. Each culture showed robust inducible and reversible expression of BE3RA (Supplementary Fig. 1a), and organoids transduced with the BE-activatable GFP^{GO} reporter[28] showed editing efficiencies ranging from 40% to 90% (Fig. 2a,b and Supplementary Fig. 1b), with minimal impact on the organoid transcriptome and no detectable off-target RNA editing observed up to 8 d on dox (Extended Data Fig. 6).

To closely assess editing dynamics, we generated multiple independent iBE^{hom} pancreatic organoid cultures carrying the *LSL-Kras*^{G12D} allele and generated *Kras*^{G12D};*p53*^{Q97X} (KP) mutant organoids by nucleofecting dox-treated cells with synthetic sgRNA and tat-Cre protein; KP cultures survive serial passaging more efficiently and expand faster than wild-type (WT) organoids, simplifying serial measurements over multiple timepoints. GFP^{GO}-transduced KP organoids showed 1–2% editing in the absence of dox but induced target editing and GFP expression

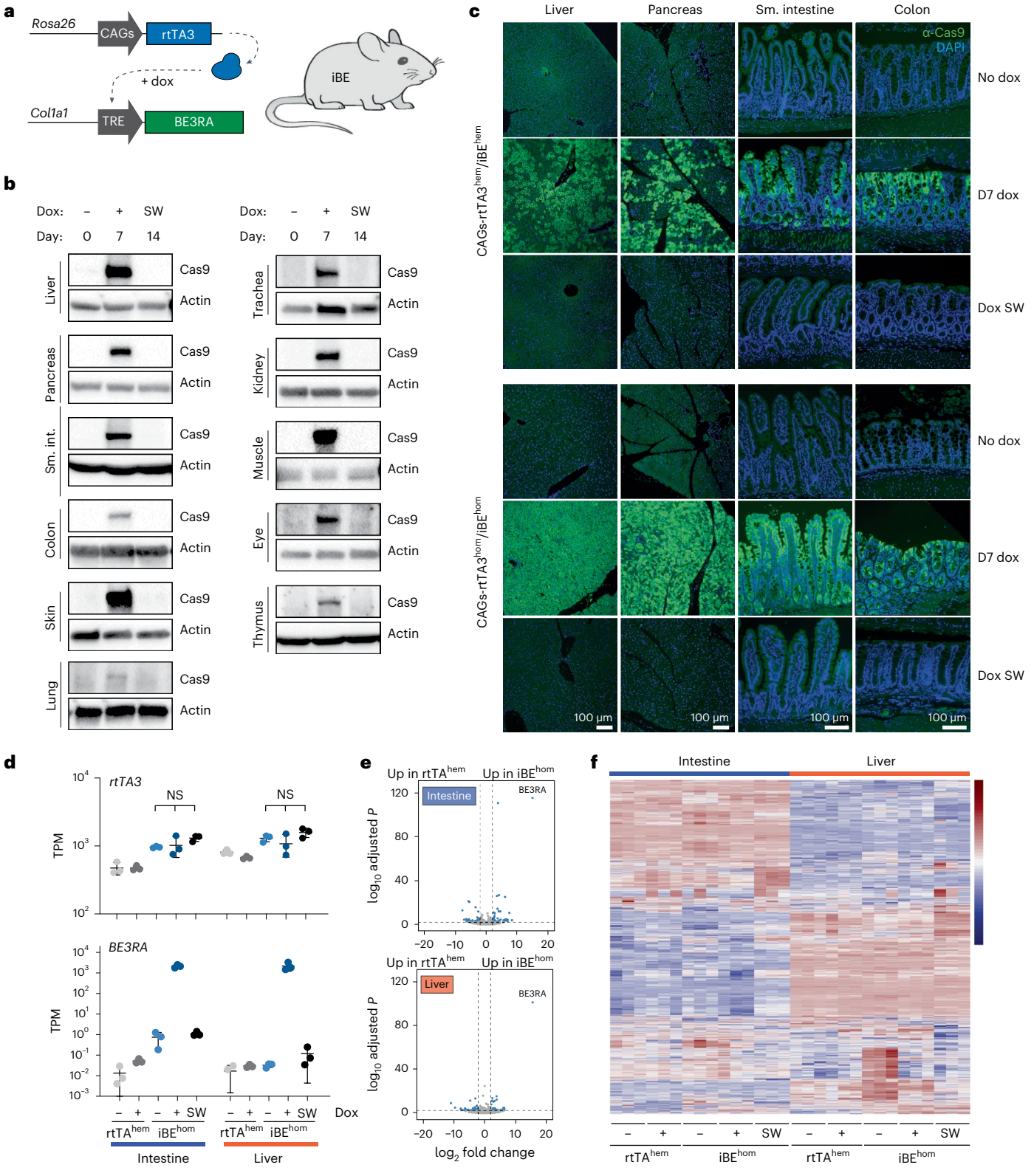

rapidly after dox treatment. Two days after dox exposure, more than 50% of cells were GFP$^+$, with maximal editing (70–80% GFP$^+$) occurring at approximately 3–4 d (Fig. 2c,d and Extended Data Fig. 7a). Transient exposure to dox for only 2 h or 12 h resulted in submaximal editing (55% and 70% of maximum, respectively), supporting the notion that BE enzyme expression and editing are both quickly induced and rapidly suppressed after dox withdrawal (Figs. 1d and 2d). Re-exposure to dox in these cells recovered maximal editing efficiency at similar kinetics to that seen in dox-naive cultures (Fig. 2d and Extended Data Fig. 7a). Consistent with the GO reporter, endogenous target editing with an Apc.Q1405-targeting sgRNA showed similar kinetics, being detectable 12 h after dox addition and reaching 80% of total BE within 48 h (Extended Data Fig. 7b). Consistent with previous experience with this sgRNA, insertions or deletions (indels) were rare at day 3 (~1% total reads) but increased four-fold when maintained on dox over 3 weeks (Extended Data Fig. 7c).

We next asked whether iBE could improve the efficiency of building complex organoid-based models of cancer. To limit the introduction of exogenous and potentially immunogenic components, we opted for transient transfection of sgRNAs by nucleofection. Organoids were cultured in dox-containing media for 2 d before and after nucleofection (4 d total) to transiently induce the editor and align BE protein expression with sgRNA expression; editing was quantified 7 d after transfection by target amplicon sequencing. Nucleofection of the *Apc*^{Q1405X} sgRNA in a U6 expression plasmid (LRT2B[8]) induced ~50% target editing, whereas *Trp53*^{Q97X} and *CR8*^{OS2} gRNAs consistently showed C > T editing below 5% (Fig. 2e). In contrast to plasmid-based delivery, nucleofection of dox-treated organoids with chemically stabilized synthetic sgRNAs led to significantly higher editing, up to 43-fold higher in the case of CR8^{OS2} (Fig. 2e and Extended Data Fig. 8a). Notably, editing with the iBE transgene was 40–100+-fold higher than nucleofection of WT organoids with synthetic sgRNAs and an optimized BE (FNLS) cDNA plasmid (Fig. 2e), highlighting the improved workflow using iBE organoids.

Using the more efficient synthetic sgRNA approach, we next tested a range of additional BE sgRNAs predicted by BE-SCAN (https://dowlab.shinyapps.io/BEscan/)[29] to effectively induce targeted SNVs. In unselected populations, 7 d after transfection, C > T editing efficiencies ranged from ~20% to 90% (Fig. 2f). Functional selection for mutant organoids (RSPO withdrawal for Ctnnb1^{S33F}, or TGFβ for Smad4^{Q224X}, Nutlin3 treatment for p53 mutations and selumetinib treatment for Pik3ca^{E545K}) enriched C > T editing 80–95% for tumor suppressor (*Smad4* and *Trp53*) and 50–80% for oncogenes (*Pik3ca* and *Ctnnb1*) (Fig. 2f and Extended Data Fig. 8b). Most guides showed minimal (bystander) editing of adjacent cytosines that would result in additional amino acid substitutions (Fig. 2g and Extended Data Figs. 8c–j and 9). The only notable exceptions to this were sgRNAs targeting *Trp53.V197M*, in which 20% of alleles carried an adjacent R196Q mutation (Extended Data Fig. 8e), and the *Trp53.Q97X* sgRNA that uniformly harbored an S96F alteration immediately before the premature termination codon (Extended Data Fig. 8c). In the latter case, the predicted functional impact on the truncated p53 protein is minimal.

Given the high efficiency of engineering individual target mutations, we next asked whether iBE organoids could be used for rapid multiplexed editing. Using iBE^{hom} organoids to maximize the likelihood of efficient enzyme expression in all cells, we delivered a combination of four sgRNAs—*Apc*^{Q1405}, *Trp53*^{C135Y}, *Smad4*^{Q224X} and *Pik3ca*^{E545K}—to model frequently observed colon cancer mutations; notably, three of the four sgRNAs used show moderate single editing efficiency (20–45%), thereby providing a test of multiplexed editing in non-ideal circumstances. Target editing for each site in the bulk, unselected populations resembled that seen with individual transfections in iBE^{hem} cells (Fig. 2h and Supplementary Fig. 2a), and iterative functional selection for each mutation resulted in an organoid population with ~80–90% C > T editing for *Apc*, *Trp53* and *Smad4* (Fig. 2i and Supplementary Fig. 2b), whereas *Pik3ca*^{E545K} editing reached ~65%, consistent with the notion that heterozygous mutations are sufficient to activate PI3K signaling. Control organoids receiving all four sgRNAs in the absence of dox showed <1% editing and did not survive functional selection (Fig. 2h and Supplementary Fig. 2a). Together, these data show that iBE provides an efficient system for engineering disease-relevant SNVs and can be used to quickly generate genetically complex cancer models.

iBE enables sequential base editing in vitro and in vivo

One powerful application of inducible BE technology is the potential for temporally separated or sequential editing. To test the feasibility of this approach, we cultured ex vivo edited, transformed *Apc*^{Q1405X}, *p53*^{C135Y}, *Smad4*^{Q224X}, *Pik3ca*^{E545K} (APSP) mutant intestinal organoids (Fig. 3a) in the absence of dox to suppress expression of the base editor and transduced the cells with the lentiviral GFP^{GO} reporter. Selected organoids maintained in the absence of dox showed minimal editing (<1%), whereas 4 d of dox treatment led to ~50% target editing (Fig. 3b,c), consistent with primary, untransformed organoids (Fig. 2a,b). To determine whether this system could be used to control the timing of gene editing in vivo, we engrafted APSP intestinal organoids into recipient animals, either subcutaneously or into the liver (via intrasplenic injection), to mimic metastatic disease (Fig. 3a). Once tumors had formed (10 d after subcutaneous transplant or 8 weeks after intrasplenic delivery), mice were treated with dox (200 mg kg^{-1} in chow) for 7 d, and tumors were collected for analysis. As expected, subcutaneous tumors expressed nuclear-localized mScarlet, whereas only the dox-treated mice showed robust GFP fluorescence throughout the tumor mass (Fig. 3d,e). Similarly, dox-treated liver 'metastases' showed

Fig. 2 | Efficient BE in ex vivo derived iBE organoids. a, Schematic of GFP^{GO} reporter and quantitation of BE-mediated GFP activation in mScarlet$^+$ organoids with and without dox by flow cytometry. **b**, Live fluorescence imaging of small intestinal and pancreatic organoids containing stable integration of GFP^{GO} lentiviral construct cultured without (no dox) or with dox. Dotted white line indicates central lumen of small intestinal organoids that produce bright autofluorescent signal. **c**, Schematic for dox treatment of KP pancreatic organoids to assess editing dynamics. **d**, Flow cytometry analysis of pancreatic KP mutant organoids integrated with GFP^{GO} reporter after: continual dox treatment (0–8 d) (black), transient exposure to dox for 12 h/2 h (gray) or transient treatment and then re-exposure to dox in the same cells (green) ($n = 3$ independently derived organoid cultures). **e**, Targeted deep sequencing quantification of target C:G to T:A conversion in small intestinal iBE organoids nucleofected with plasmid (light blue) or synthetic (indigo) gRNAs (ApcQ1405, Trp53Q97, CR8.OS2) as indicated and WT organoids nucleofected with synthetic sgRNAs and an optimized BE (FNLS) cDNA plasmid (orange). **f**, Targeted deep sequencing quantification of target C:G to T:A conversion in dox-treated small intestinal iBE organoids nucleofected with various synthetic gRNAs as indicated and either unselected (−) or selected with corresponding functional selective media condition. **g**, Frequency of precise amino acid substitution in small intestinal iBE organoids nucleofected with synthetic gRNAs in **f**. **h**, Bright-field images of small intestinal iBE organoids targeted with various gRNA combinations and dox conditions (left) taken through sequential selection of RSPOI withdrawal, Nutlin3, TGFβ and selumetinib. Bolded black boxes are conditions failing to survive selection. Bolded green boxes indicate quadruple targeted organoids (with dox) surviving all four selection conditions. Images are representative of three independently derived intestinal organoid cultures. **i**, Targeted deep sequencing quantification of target C:G to T:A conversion (and C> other or indels) in small intestinal iBE organoids nucleofected with four synthetic gRNAs in **e** (green boxes) at each gRNA target loci (ApcQ1405, Trp53C135, Smad4Q224, Pik3caE545). Media conditions and corresponding organoid genotype and sequencing information are grouped and listed above ($n = 3$, P values derived from one-way ANOVA with Tukey's correction for multiple testing). All data are presented as mean values ± s.e.m. All experiments describing iBE organoids include three independently derived organoid cultures.

https://doi.org/10.1038/s41587-023-01900-x

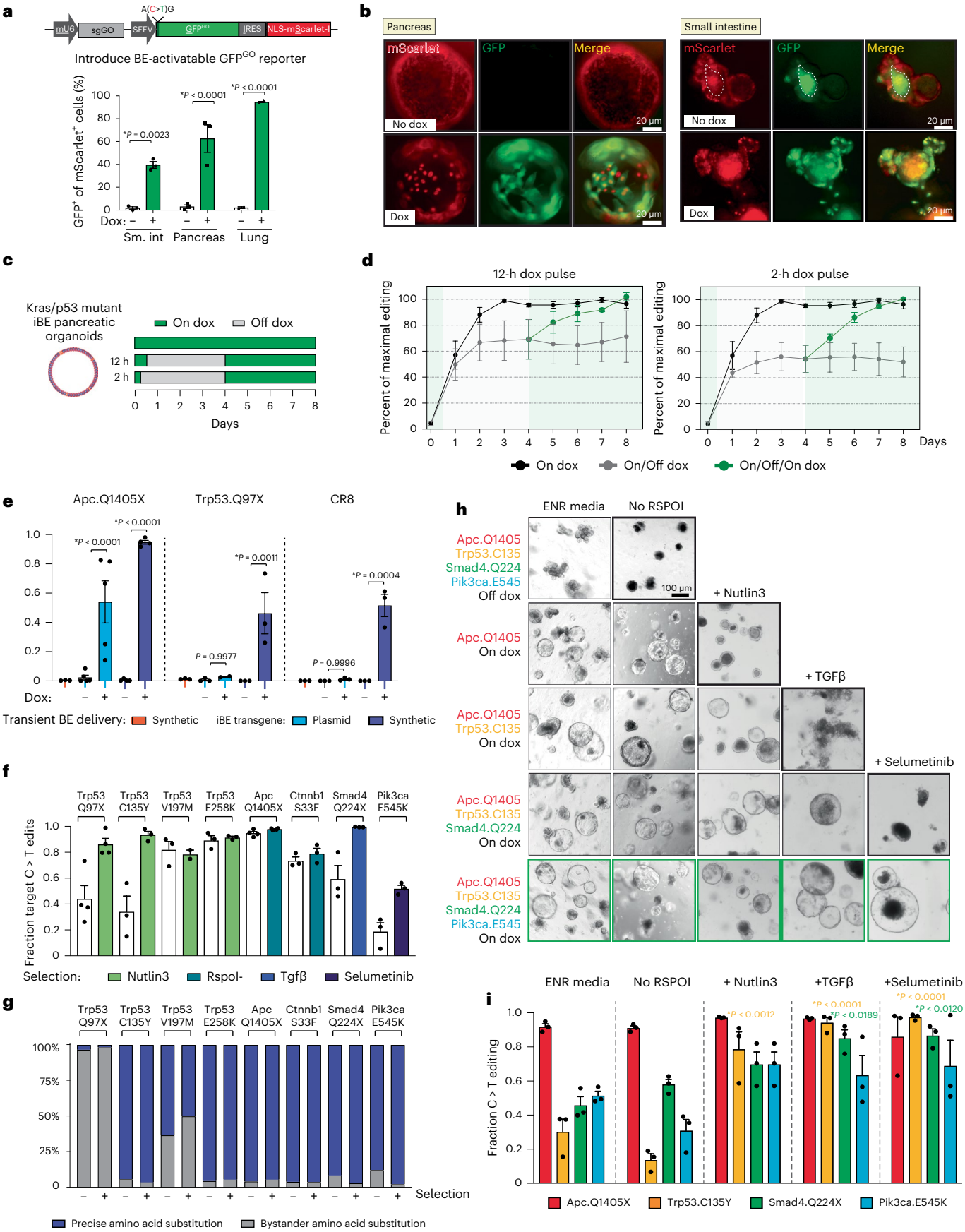

https://doi.org/10.1038/s41587-023-01900-x

widespread GFP activation compared to non-dox-treated control animals (Fig. 3g). Flow cytometry analysis showed editing efficiencies up to 40%, with low levels of leaky GFP activation, even after 8 weeks of in vivo tumor growth (Fig. 3f,h).

iBE enables precise somatic editing in the liver

We and others previously used transfection and viral-based delivery of base editors to generate somatic mutations in mouse hepatocytes, in situ[8,13–20]. Although remarkably effective in liver, somatic

https://doi.org/10.1038/s41587-023-01900-x

Fig. 3 | iBE enables sequential BE in vitro and in vivo. a, Schematic representation of the experimental workflow for sequential BE in vivo. WT small intestinal organoids were isolated from iBE^{hom} mice and treated with dox to induce the BE alongside with synthetic sgRNA to engineer four oncogenic SNVs (as shown in Fig. 2h). Dox was withdrawn to silence BE transgene expression, and a fifth sgRNA was introduced in a lentiviral vector carrying the GFP^{GO} fluorescent BE reporter. Organoids were engrafted into the flanks or livers of recipient mice, and tumors were allowed to form 10 d for subcutaneous injection or 8 weeks for liver engraftment. Mice were treated with systemic dox (in the chow) for 1 week to induce BE expression. **b**, Fluorescence imaging of quadruple mutant small intestine organoids containing stable integration of GFP^{GO} reporter cultured without (no dox) or with dox. **c**, Quantification by flow cytometry of GFP^{GO} activation in mScarlet^{+} organoids with and without dox from **b**. Data are presented as mean values ± s.e.m. ($n = 5$ mice per condition) (*$P < 0.05$, Student's *t*-test, unpaired, two-sided). **d**, In vivo fluorescence imaging of mice containing subcutaneous tumors maintained on normal chow (no dox) or dox chow for 7 d (day 7 dox). **e**, Immunohistochemical detection of GFP and mScarlet in subcutaneous tumors harvested from mice maintained on normal chow (no dox) or dox chow for 7 d (day 7 dox). **f**, Quantification by flow cytometry of GFP^{GO} activation in enzymatically digested subcutaneous tumors with and without dox. Data are presented as mean values ± s.e.m. ($n = 5$ mice per condition) (*$P < 0.05$, Student's *t*-test, unpaired, two-sided). **g**, Whole-mount fluorescence, H&E and immunohistochemical detection of GFP and mScarlet in liver tumors harvested from mice maintained on normal chow (no dox) or dox chow for 7 d (day 7 dox). **h**, Quantification by flow cytometry of GFP^{GO} activation in dissected and enzymatically digested liver tumors from **g**. Data are presented as mean values ± s.e.m. ($n = 5$ mice per condition) (*$P < 0.05$, Student's *t*-test, unpaired, two-sided). D, day.

delivery of Cas9-based enzymes can result in antigen-mediated immune responses[30–32]. As a first step to measure whether in vivo somatic editing with the iBE allele could be used to derive tumor models, we used hydrodynamic tail vein injection (HTVI) to introduce a *Myc* cDNA in a sleeping beauty (SB) cassette (*SB-Myc*) as well as sgRNAs targeting *Apc*, *Ctnnb1* or *Trp53* designed to engineer known cancer-linked SNVs[8,33,34]. To drive BE enzyme expression, iBE mice were maintained on dox for 1 week before injection and for 1 week after injection (Fig. 4a). Six weeks after HTVI, tissue was harvested for sequencing and histological analysis (Fig. 4a). Most mice (12/13) injected with SB-*Myc* and a control sgRNA targeting a non-genic region (CR8) had no macroscopically visible tumors but showed small, well-circumscribed regions on histological sections, which were also observed in *SB-Myc*-only animals (Fig. 4b). Consistent with an established role for WNT signaling in a subset of HCC[8,33,34], *SB-Myc;Apc*^{Q1405X} and *SB-Myc;Ctnnb1*^{S33F} mice showed markedly enhanced tumor growth (5/6 and 4/6 mice, respectively) (Fig. 4b). Targeted amplicon sequencing revealed a high proportion of expected SNVs, with low rates of indels (Supplementary Fig. 3a–e). Absolute editing rates in bulk tumor tissue were variable, likely due to the presence of admixed stroma and immune cells (Fig. 4c and Supplementary Fig. 3a–c). Notably, *SB-Myc;Ctnnb1*^{S33F} tumors showed lower overall editing rates than *Apc*^{Q1405X} mutant tumors, consistent with the notion that heterozygous *Ctnnb1*^{S33F} mutations are sufficient to activate WNT signaling, whereas *Apc* requires inactivation of both alleles. Both *Apc*^{Q1405X} and *Ctnnb1*^{S33F} tumors showed accumulation and mislocalization of β-catenin protein and elevated expression of glutamine synthetase (GS), a WNT target that is normally restricted to pericentral hepatocytes surrounding the central vein (Fig. 4b). Consistent with a strong tumor-suppressive role for p53 in HCC, introduction of an sgRNA targeting *Trp53* (Trp53.C135Y) accelerated tumor growth, with five of seven mice showing multi-focal tumors and high levels of on-target editing (Fig. 4b,c and Supplementary Fig. 3d). Like previously characterized p53 hotspot mutations[35–38], C135Y resulted in p53 protein stabilization and nuclear localization (Fig. 4b,c and Supplementary Fig. 3d). Interestingly, despite detectable editing within macroscopic tumor nodules (Fig. 4b), most M237I sgRNA-transfected livers showed small lesions resembling those seen with Myc alone, with isolated regions of each tumor showing elevated nuclear staining for p53 (Fig. 4b).

Given the reduced tumor penetrance in Myc/p53^{M237I} transfected livers, we asked whether addition of a second oncogenic mutation could be combined to enable tumor growth with this p53 alteration. Delivery of two sgRNAs (*Trp53*^{M237I} and *Ctnnb1*^{S33F}) drove tumor growth in all mice analyzed (4/4) with detectable editing in both target loci. These tumors showed increased CTNNB1 protein and WNT target (GS) expression. Like M237I alone, dual-edited tumors showed sporadic nuclear p53 staining (Fig. 4e,d and Supplementary Fig. 4). To confirm that the editing of both loci was occurring within the same cells of the tumor, we derived four cell lines from individual tumor nodules from two different animals. This analysis revealed editing and mutational activation of β-catenin in each of the four cell lines, with tumor line 4 showing a non-canonical C > A conversion, consistent with the frequency of editing outcomes seen previously with this sgRNA (Fig. 4f)[28]. Two of four lines contained homozygous p53^{M237I} editing, whereas the remaining two showed heterozygous p53^{M237I} alterations, in line with reduced editing observed in single sgRNA experiments and perhaps explaining the variability of nuclear p53 staining (Supplementary Fig. 4).

In an effort to improve the efficiency of developing in vivo models with iBE and to eliminate the need for sgRNA cloning, we tested the delivery of chemically stabilized, non-encapsulated ('naked') synthetic sgRNAs. Like plasmid delivery, synthetic sgRNAs targeting *Apc*, *Ctnnb1* or *Trp53* coupled with *SB-Myc* drove consistent tumor formation in the liver after HTVI (Extended Data Fig. 10a,b). For both nonsense (*Apc*^{Q1405X} and *Trp53*^{Q97X}) and missense (*Ctnnb1*^{S33F}) mutations, we saw high on-target C > T editing and low indel formation (Supplementary Fig. 3g–i).

Together, these data show that the iBE mouse enables temporally regulated target editing and can be used to generate in vivo liver cancer models through controlled and precise induction of cancer-relevant SNVs.

Engineering oncogenic missense mutations in the pancreas

To test the potential for using iBE in the generation of in situ cancer models in tissue other than liver, we used an electroporation-based approach[39,40] to introduce a targeted mutation into the mouse pancreas combined with an SB cassette that expresses Kras^{G12D} (*SB-Kras*) (Fig. 5a).

Fig. 4 | In situ BE with iBE drives liver tumors. a, Schematic for experimental setup of HTVI-mediated delivery of plasmid gRNA and SB transposon-mediated integration of cMyc cDNA (SB-Myc) in the liver of iBE mice maintained on dox for 1 week surrounding injection. After injection, mice are monitored for tumor development, and palpable tumors are harvested for tumor histological and sequencing analysis. **b**, Bright-field images of liver after harvest targeted according to the experimental pipeline in **a** and with the corresponding gRNA listed (top). H&E staining (second row) of corresponding liver lesions. Immunohistochemical staining of total β-catenin (green, third row), GS (red, fourth row) and p53 (black, fifth row). Fraction of number of mice with palpable tumors over number of mice injected is below each column. **c**,**d**, Targeted deep sequencing analysis of target C:G to T:A conversion in individual dissected tumors collected in **b** for individual (**c**) or multiplexed (**d**) experiments. Each point corresponds to a physically isolated individual bulk tumor ($n = 3$ mice minimum for a given gRNA target). Individual editing data color-coded by animal are shown in Supplementary Fig. 3. Data are presented as mean values ± s.e.m. **e**, Bright-field images of liver after multiplexed delivery of SB-Myc and both Trp53^{M237I} and Ctnnb1^{S33F} sgRNAs. **f**, Sequencing of target sites of cell lines derived from individual liver tumor isolated from mice targeted with both Ctnnb1^{S33F} and Trp53^{M237I}. Predicted translation of sequenced regions is shown below with WT amino acid (gray) and targeted amino acid substitution for Ctnnb1 (blue) and Trp53 (orange).

https://doi.org/10.1038/s41587-023-01900-x

iBE^{hem} mice targeted with *Trp53* gRNAs showed rare incidence of tumor development (1/10 mice); however, iBE^{hom} mice showed induction of large pancreatic tumors in four of seven mice by 5–8 weeks (Fig. 5b and Supplementary Fig. 5a,b). Like genetically engineered Kras;p53-driven Cre models[35], tumors contained cytokeratin-19-positive ductal islands with substantial surrounding stroma expressing alpha-smooth muscle

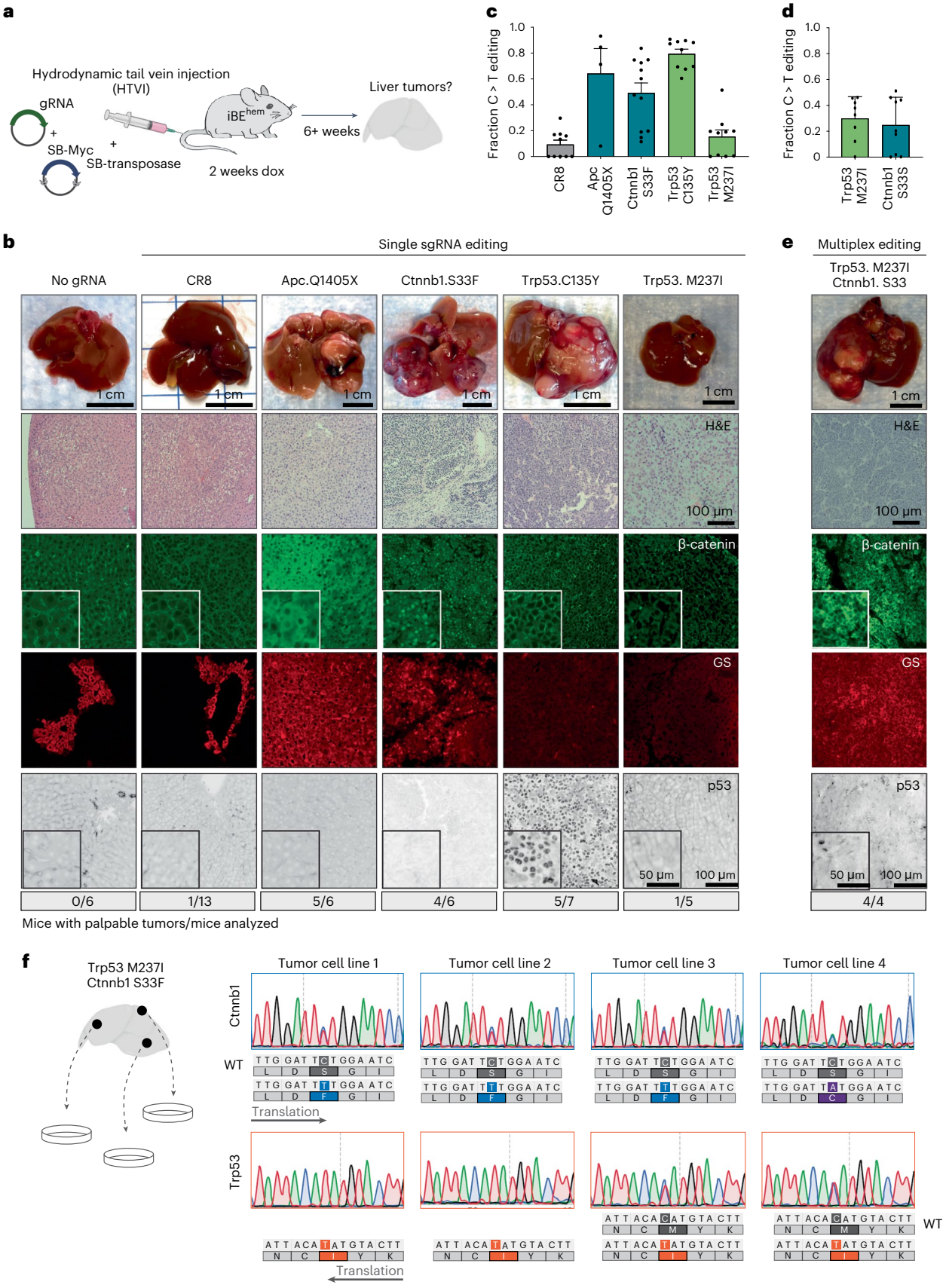

https://doi.org/10.1038/s41587-023-01900-x

actin (Fig. 5b). Sequencing of bulk tumors revealed precise on-target C > T editing with minimal indels. Absolute editing percentages from bulk tumor were low, likely due to the abundance of non-tumor cells, as frequently observed in human and mouse PDAC (Fig. 5c). Electroporation of the pancreas with SB-*Kras*^{G12D} and synthetic *Trp53.Q97X* sgRNAs in iBE^{hom} mice showed highly penetrant tumor growth (5/6 mice), efficient C > T editing and identical histology to what was observed with plasmid-based delivery (Fig. 5c and Supplementary Fig. 5b,c). Finally, following the same paradigm used previously in the liver, we generated genetically complex PDACs in vivo by multiplexed delivery of *SB-Kras* and sgRNAs targeting both *Trp53.Q97* and *Pik3ca.E545* (Fig. 5d). All tumors showed evidence of editing at both target sites, at levels consistent with that observed for individual sgRNAs (Fig. 5e and Supplementary Fig. 5d,e). Moreover, dual *Trp53*^{Q97X} and *Pik3ca*^{E545K} edited tumors showed elevated levels of pAKT compared to *Trp53*^{Q97X} only tumors, consistent with mutation-driven activation of the PI3K/AKT pathway (Fig. 5f). Thus, iBE mice provide a platform for rapid and easy generation of disease-associated SNVs in multiple organ sites in situ.

Discussion

The generation of model systems that faithfully recapitulate the genetic alterations observed in human disease is a key step in developing precision treatment strategies. In this study, we set out to produce an efficient and regulated platform to streamline the creation of such preclinical disease models. The iBE platform enables efficient creation of targeted nonsense and missense mutations in vivo in somatic tissues and in cells and organoids derived from mice. Furthermore, the system supports multiplexed and/or sequential editing with synthetic sgRNAs, thus providing a rapid approach to engineer complex genetic combinations often seen in human cancers.

Previous work demonstrated the potential of in vivo BE for engineering SNVs[8,13–20], although these approaches have relied on exogenous delivery of BE enzymes using transfection, split inteins in adeno-associated virus vectors or engineered virus-like particles. These approaches can catalyze highly efficient editing in a subset of tissues (that is, the liver, muscle, brain and eye)[8,13–20], although they may suffer from unintended immune recognition of Cas9-derived antigens[30–32]. iBE broadens the number of tissues that can be targeted with cytosine BE for disease modeling and, as it is encoded in the genome, may avoid complications of immunogenicity when induced in somatic tissues. We cannot rule out a potential immune response to exogenously delivered sgRNA expression vectors or even naked sgRNA, although, to our knowledge, such responses have not been reported. Annunziato et al.[41] previously described a genomically encoded Cre-activatable BE mouse using the pre-optimized BE3 enzyme. This transgenic mouse demonstrated the ability to induce target editing in the mammary gland and drive tumor development in combination with Myc; however, perhaps due to the sustained expression of BE3 from a constitutive promoter, target sites often accumulated indels rather than desired SNVs[41]. In the present study, we saw minimal indel formation across 10 different target sites both in vitro and in vivo. However, as expected, we saw a modest accumulation of indels in cells maintained on dox over 3 weeks in culture. Thus, the reversible induction of enzyme expression in iBE provides a key improvement that limits indel formation at endogenous genomic targets.

Our goal was to develop a system for creating precise, genetically defined preclinical models. One recent study described the generation of constitutive BE3 transgenic mice using *piggybac* transposition

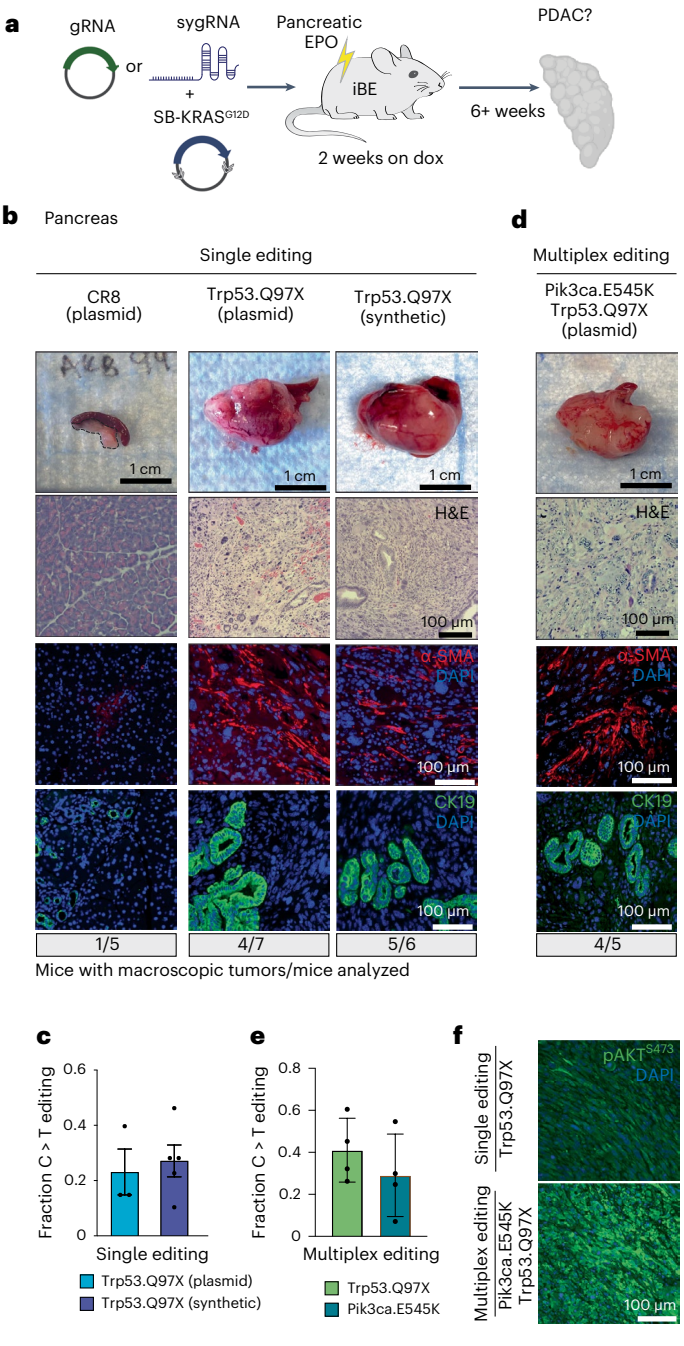

Fig. 5 | Efficient engineering of missense mutations in pancreatic tumor models. a, Schematic for experimental setup of pancreatic electroporation (EPO)-mediated delivery of plasmid-based (gRNA) or synthetic (sygRNA) guide RNAs and SB transposon-mediated integration of KrasG12D cDNA (SB-Kras) in the pancreas of iBE^{hom} mice maintained on dox for 2 weeks surrounding electroporation. After electroporation, mice are monitored for tumor development, and palpable tumors are harvested for tumor histological and sequencing analysis. **b**, Bright-field images of pancreas tumor with spleen attached (top row) using plasmid or synthetic gRNA. H&E staining (second row) of pancreatic tumors electroporated as in **a** for gRNAs listed. Immunohistochemical staining of α-SMA (red, third row) and CK19 (green, fourth row) counterstained with DAPI (blue). Number of mice with palpable tumors over number of mice injected is below each column. **c**, Targeted deep sequencing analysis of target C:G to T:A conversion in tumors collected in **b** for plasmid gRNA (left) and synthetic gRNA (right). Each point corresponds to one mouse analyzed ($n = 3$ mice minimum for a given gRNA target). Data are presented as mean values ± s.e.m. **d**, Bright-field images of pancreas tumor with spleen attached (top row) using plasmid gRNA targeting both Trp53Q97X and Pik3caE545. **e**, Targeted deep sequencing analysis of target C:G to T:A conversion in pancreatic tumors collected using plasmid gRNA targeting both Trp53Q97X and Pik3caE545. Each point corresponds to one mouse analyzed ($n = 4$). Data are presented as mean values ± s.e.m. **f**, Immunohistochemical staining of pAKT^{S473} in pancreatic tumors using gRNA targeting Trp53Q97X alone or both Trp53Q97X and Pik3caE545. Image shown is representative of $n = 4$ independent tumors analyzed.

and reported high levels of off-target DNA and RNA editing throughout the genome and transcriptomes of these mice, respectively[24]. We thoroughly explored sequence-independent DNA and RNA off-target effects after dox induction in iBE cells and tissues. Rather than performing whole-genome sequencing on a small number of post-editing clones, we opted for targeted deep sequencing of cancer-relevant genes contained in the MSK-IMPACT panel[25]. Although this approach does not measure editing across the entire genome, it enabled the analysis of 120 individual ESC clones. We saw no increase in APOBEC-mediated (C > T) mutation profile in dox-treated samples, suggesting that iBE does not induce widespread sequence-independent DNA off-targets in cancer-associated genes, but we cannot rule out the possibility of rare mutations elsewhere in the genome. It is likely that limiting dox exposure through transient induction of the editing enzyme avoids many of the unwanted genomic edits described in other studies.

Similarly, and in contrast to published data[23,42], we saw no evidence of sequence-independent off-target RNA editing in pancreatic organoids on dox for 8 d and only 3–6-fold increase in RNA variants in intestinal and liver tissue from mice treated with dox for 2 weeks. In fact, RNA editing in iBE mice was 10-fold lower than reported by Yan et al.[24] and 100-fold lower than observed in HEK293 transfected cells[23] (Extended Data Fig. 4). As described for off-target DNA editing, we think it is likely that the relatively modest level of enzyme expression from the single-copy transgene can maintain on-target DNA editing while minimizing potential off-target effects (Supplementary Fig. 4). Moreover, withdrawal of dox for 6 d in iBE animals reversed already low RNA editing to baseline levels, implying that the observed editing was not reflective of permanent DNA mutagenesis but is transient and can be minimized through shortening the window of BE enzyme induction. Together, these observations suggest that most reported off-target consequences of BE enzymes can be mitigated by carefully regulating the duration and absolute level of BE enzyme expression, highlighting the utility of iBE mice for preclinical disease modeling.

Accurate genetic disease modeling in the mouse involves both targeting the correct cell populations and engineering precise genomic changes in those cells. In this study, we used iBE animals in which expression of the BE enzyme was induced throughout the body and restricted delivery of the sgRNAs to specific tissues. In situations where sgRNA delivery cannot be directed to a specific tissue or cell population of interest, induction of the BE enzyme can be restricted to specific compartments by combining iBE with well-characterized cell or tissue-restricted rtTA or Cre drivers. This would enable broad delivery of sgRNAs (for example, via adeno-associated virus) by restricting editing to those cells expressing the BE transgene. To produce precise SNVs or single amino acid substitutions, sgRNA selection is critical. We used a range of sgRNAs from a pre-validated collection[29] that estimates editing purity. As shown in Fig. 2, in most cases, it is possible to achieve highly precise target editing in bulk populations, but the use of prediction tools[43–46] or empirically tested collections[29,47] will help maximize efficiency and minimize unwanted bystander editing. There will be situations in which the presence of adjacent cytosines restricts the ability of iBE to produce single precise amino acid changes. Furthermore, although C > T mutations represent the most frequent cancer-associated variants, specific disease models may require different base substitutions. In these cases, the use of genome editing approaches, such as in vivo homology-directed repair (HDR)[48] or prime editing[49,50], provide a strategy to overcome the limitations of BE, although increased flexibility may come at a cost of targeting efficiency.

Our proof-of-concept studies demonstrate the utility of the iBE platform for ex vivo and in vivo target editing. Furthermore, given the broad expression of iBE across all tested tissues, and the ability to control timing and tissue distribution of BE activity, the model is a powerful tool to engineer and study missense mutation in vivo for many disease applications.

Online content

Any methods, additional references, Nature Portfolio reporting summaries, source data, extended data, supplementary information, acknowledgements, peer review information; details of author contributions and competing interests; and statements of data and code availability are available at https://doi.org/10.1038/s41587-023-01900-x.

References

1. Goodwin, S., McPherson, J. D. & McCombie, W. R. Coming of age: ten years of next-generation sequencing technologies. *Nat. Rev. Genet.* **17**, 333–351 (2016).
2. Landrum, M. J. et al. ClinVar: public archive of interpretations of clinically relevant variants. *Nucleic Acids Res.* **44**, D862–D868 (2016).
3. Vogelstein, B. et al. Cancer genome landscapes. *Science* **339**, 1546–1558 (2013).
4. Vivanco, I. et al. Differential sensitivity of glioma- versus lung cancer-specific EGFR mutations to EGFR kinase inhibitors. *Cancer Discov.* **2**, 458–471 (2012).
5. Hyman, D. M. et al. AKT inhibition in solid tumors with *AKT1* mutations. *J. Clin. Oncol.* **35**, 2251–2259 (2017).
6. Vasan, N. et al. Double *PIK3CA* mutations in cis increase oncogenicity and sensitivity to PI3Kα inhibitors. *Science* **366**, 714–723 (2019).
7. Findlay, G. M. et al. Accurate classification of *BRCA1* variants with saturation genome editing. *Nature* **562**, 217–222 (2018).
8. Zafra, M. P. et al. Optimized base editors enable efficient editing in cells, organoids and mice. *Nat. Biotechnol.* **36**, 888–893 (2018).
9. Komor, A. C., Kim, Y. B., Packer, M. S., Zuris, J. A. & Liu, D. R. Programmable editing of a target base in genomic DNA without double-stranded DNA cleavage. *Nature* **533**, 420–424 (2016).
10. Gaudelli, N. M. et al. Programmable base editing of A•T to G•C in genomic DNA without DNA cleavage. *Nature* **551**, 464–471 (2017).
11. Gaudelli, N. M. et al. Directed evolution of adenine base editors with increased activity and therapeutic application. *Nat. Biotechnol.* **38**, 892–900 (2020).
12. Komor, A. C. et al. Improved base excision repair inhibition and bacteriophage Mu Gam protein yields C:G-to-T:A base editors with higher efficiency and product purity. *Sci. Adv.* **3**, eaao4774 (2017).
13. Rothgangl, T. et al. In vivo adenine base editing of *PCSK9* in macaques reduces LDL cholesterol levels. *Nat. Biotechnol.* **39**, 949–957 (2021).
14. Villiger, L. et al. In vivo cytidine base editing of hepatocytes without detectable off-target mutations in RNA and DNA. *Nat. Biomed. Eng.* **5**, 179–189 (2021).
15. Villiger, L. et al. Treatment of a metabolic liver disease by in vivo genome base editing in adult mice. *Nat. Med.* **24**, 1519–1525 (2018).
16. Song, C.-Q. et al. Adenine base editing in an adult mouse model of tyrosinaemia. *Nat. Biomed. Eng.* **4**, 125–130 (2019).
17. Yeh, W. H., Chiang, H., Rees, H. A., Edge, A. S. B. & Liu, D. R. In vivo base editing of post-mitotic sensory cells. *Nat. Commun.* **9**, 2184 (2018).
18. Banskota, S. et al. Engineered virus-like particles for efficient in vivo delivery of therapeutic proteins. *Cell* **185**, 250–265 (2022).
19. Ryu, S. M. et al. Adenine base editing in mouse embryos and an adult mouse model of Duchenne muscular dystrophy. *Nat. Biotechnol.* **36**, 536–539 (2018).
20. Yang, L. et al. Amelioration of an inherited metabolic liver disease through creation of a de novo start codon by cytidine base editing. *Mol. Ther.* **28**, 1673–1683 (2020).
21. Dow, L. E. et al. Conditional reverse tet-transactivator mouse strains for the efficient induction of TRE-regulated transgenes in mice. *PLoS ONE* **9**, e95236 (2014).

22. Premsrirut, P. K. et al. A rapid and scalable system for studying gene function in mice using conditional RNA interference. *Cell* **145**, 145–158 (2011).
23. Grunewald, J. et al. CRISPR DNA base editors with reduced RNA off-target and self-editing activities. *Nat. Biotechnol.* **37**, 1041–1048 (2019).
24. Yan, N. et al. Cytosine base editors induce off-target mutations and adverse phenotypic effects in transgenic mice. *Nat. Commun.* **14**, 1784 (2023).
25. Zehir, A. et al. Mutational landscape of metastatic cancer revealed from prospective clinical sequencing of 10,000 patients. *Nat. Med.* **23**, 703–713 (2017).
26. Zafra, M. P. et al. An in vivo *Kras* allelic series reveals distinct phenotypes of common oncogenic variants. *Cancer Discov.* **10**, 1654–1671 (2020).
27. Schatoff, E. M. et al. Distinct CRC-associated APC mutations dictate response to tankyrase inhibition. *Cancer Discov.* **9**, 1358–1371 (2019).
28. Katti, A. et al. GO: a functional reporter system to identify and enrich base editing activity. *Nucleic Acids Res.* **48**, 2841–2852 (2020).
29. Sanchez-Rivera, F. J. et al. Base editing sensor libraries for high-throughput engineering and functional analysis of cancer-associated single nucleotide variants. *Nat. Biotechnol.* **40**, 862–873 (2022).
30. Mehta, A. & Merkel, O. M. Immunogenicity of Cas9 protein. *J. Pharm. Sci.* **109**, 62–67 (2020).
31. Chew, W. L. et al. A multifunctional AAV–CRISPR–Cas9 and its host response. *Nat. Methods* **13**, 868–874 (2016).
32. Wang, D. et al. Adenovirus-mediated somatic genome editing of *Pten* by CRISPR/Cas9 in mouse liver in spite of Cas9-specific immune responses. *Hum. Gene Ther.* **26**, 432–442 (2015).
33. Ruiz de Galarreta, M. et al. β-catenin activation promotes immune escape and resistance to anti-PD-1 therapy in hepatocellular carcinoma. *Cancer Discov.* **9**, 1124–1141 (2019).
34. Calvisi, D. F. et al. Activation of the canonical Wnt/β-catenin pathway confers growth advantages in c-Myc/E2F1 transgenic mouse model of liver cancer. *J. Hepatol.* **42**, 842–849 (2005).
35. Hingorani, S. R. et al. *Trp53R172H* and *KrasG12D* cooperate to promote chromosomal instability and widely metastatic pancreatic ductal adenocarcinoma in mice. *Cancer Cell* **7**, 469–483 (2005).
36. Alsner, J. et al. A comparison between p53 accumulation determined by immunohistochemistry and *TP53* mutations as prognostic variables in tumours from breast cancer patients. *Acta Oncol.* **47**, 600–607 (2008).
37. Freed-Pastor, W. A. & Prives, C. Mutant p53: one name, many proteins. *Genes Dev.* **26**, 1268–1286 (2012).
38. Bartek, J., Iggo, R., Gannon, J. & Lane, D. P. Genetic and immunochemical analysis of mutant p53 in human breast cancer cell lines. *Oncogene* **5**, 893–899 (1990).
39. Maresch, R. et al. Multiplexed pancreatic genome engineering and cancer induction by transfection-based CRISPR/Cas9 delivery in mice. *Nat. Commun.* **7**, 10770 (2016).
40. Park, J. S. et al. Pancreatic cancer induced by in vivo electroporation-enhanced sleeping beauty transposon gene delivery system in mouse. *Pancreas* **43**, 614–618 (2014).
41. Annunziato, S. et al. In situ CRISPR–Cas9 base editing for the development of genetically engineered mouse models of breast cancer. *EMBO J.* **39**, e102169 (2020).
42. Zhou, C. et al. Off-target RNA mutation induced by DNA base editing and its elimination by mutagenesis. *Nature* **571**, 275–278 (2019).
43. Arbab, M. et al. Determinants of base editing outcomes from target library analysis and machine learning. *Cell* **182**, 463–480 (2020).
44. Marquart, K. F. et al. Predicting base editing outcomes with an attention-based deep learning algorithm trained on high-throughput target library screens. *Nat. Commun.* **12**, 5114 (2021).
45. Pallaseni, A. et al. Predicting base editing outcomes using position-specific sequence determinants. *Nucleic Acids Res.* **50**, 3551–3564 (2022).
46. Park, J. & Kim, H. K. Prediction of base editing efficiencies and outcomes using DeepABE and DeepCBE. *Methods Mol. Biol.* **2606**, 23–32 (2023).
47. Kim, Y. et al. High-throughput functional evaluation of human cancer-associated mutations using base editors. *Nat. Biotechnol.* **40**, 874–884 (2022).
48. Winters, I. P. et al. Multiplexed in vivo homology-directed repair and tumor barcoding enables parallel quantification of Kras variant oncogenicity. *Nat. Commun.* **8**, 2053 (2017).
49. Bock, D. et al. In vivo prime editing of a metabolic liver disease in mice. *Sci. Transl. Med.* **14**, eabl9238 (2022).
50. Davis, J. R. et al. Efficient prime editing in mouse brain, liver and heart with dual AAVs. *Nat. Biotechnol.* https://doi.org/10.1038/s41587-023-01758-z (2023).

Methods

Animals

All animal experiments were approved by the Weill Cornell Medicine Institutional Animal Care and Use Committee (IACUC) under protocol 2014-0038 or by the Memorial Sloan Kettering Cancer Center (MSKCC) IACUC under protocol 11-06-018. ESC-derived mice were produced by injection into albino B6 blastocyst by the transgenic targeting core facility at New York University School of Medicine. High chimera (agouti) founders were backcrossed to C57Bl/6 mice for at least four generations before analysis. iBE^{het} mice were generated through breeding with C57Bl/6 mice containing a R26-CAGs-rtTA3 allele (Supplementary Table 1). iBE^{hom} mice were generated through breeding iBE^{het} progeny. Animals will be made available at Jackson Laboratory under strain designation B6.Cg-*Col1a1*$^{tm1(tetO\text{-}cas9^{*})Ldow}$/Mmjax (JR037818). Mice were genotyped by Col1a1 (ref. 51), R26 and CAGs-rtTA3 PCRs using EconoTaq PLUS (Lucigen, 30033-2). Dox chow (food pellets) were administered for 1 week or 2 weeks (as specified) at 200 mg kg^{-1} (Envigo, TD.180625). Mice were manipulated experimentally (organoids, injection or electroporation) at 8–12 weeks of age. Male and female mice were used for all studies.

Cloning

All plasmid sgRNAs were cloned into the BsmBI site of LRT2B[8]. Oligos for gRNA cloning are listed in Supplementary Table 4.

ESC targeting

KH2 mouse ESCs harboring a TRE-BE3RA transgene at the Col1a1 locus were engineered as previously described[8]. In brief, the BE3RA cDNA from Lenti-BE3RA was cloned into the *Col1a1* targeting vector containing a TRE promoter element (cT)[51].

TaqMan copy number assay

After gDNA isolation using the Qiagen blood and tissue kit, copy number assays were performed using the TaqMan Copy Number Assay (Thermo Fisher Scientific, 4400291) following the manufacturer's instructions.

Cells

HEK293T (American Type Culture Collection (ATCC), CRL-3216) cells were purchased from ATCC. Stocks were tested for mycoplasma routinely every 6 months and maintained in DMEM (Corning, 10-013-CV) containing 1% Pen/Strep (Corning, 30-002-Cl) and 10% FBS at 37 °C with 5% CO_2.

Organoid culture and transduction

Murine small intestine organoids from the indicated genotypes were isolated and maintained as previously described[52]. Isolation of murine pancreatic ductal organoids was done by modifying a previously described protocol[53,54]. Isolation of murine pulmonary basal cell spheroids was performed using tracheas pooled from three animals. Animals were killed by inhaled carbon dioxide, sprayed down with 70% ethanol and then sheathed. After gross dissection of the thoracic cavity, animals were cardiac perfused with PBS through the left ventricle, and tracheas were cut away from the bronchial tree, capping at the submucosal glands. Single-cell suspensions were generated using a gentleMACS Octo Dissociator and a mouse lung dissociation kit (Miltenyi Biotec, 30-095-927) on the m_lung_02 protocol. Crude suspensions were then passed through 70-µm mesh filters and rinsed with 10 cc of cold FACS buffer (PBS + 2% FBS + 2 mM EDTA). Cells were pelleted at 500*g* for 3 min, and red blood cells were lysed for 3 min using 5 cc of ACK lysis buffer (Thermo Fisher Scientific, A1049201) and then quenched with 20 cc of FACS buffer. Cell pellets were resuspended in FACS buffer, filtered through 70-µm cell strainer FACS tubes and counted (Nexcelom Cellometer Auto X4). Cd31/Cd45 cells were depleted using 10 µl each of Cd31 (Miltenyi Biotec, 130-097-418) and Cd45 (Miltenyi Biotec, 130-052-301) microbeads per 10^7 total cells and passed through an LD depletion column (Miltenyi Biotec, 130-042-901). Cells were seeded in a 6.5-mm transwell insert at ~20,000 cells in 200 µl of a 50% Matrigel suspension (BD Biosciences, 354230) per transwell. Matrigel/cell mix was incubated for 15 min at 37 °C to allow for solidification, and base media with Primocin (InvivoGen) was added to the top and bottom chambers of the transwell. Base media constitutes: DMEM/F12 + HEPES (15 mM) + sodium bicarbonate (3.6 mM) + L-glutamine (4 mM) + insulin (10 µg ml^{-1}) + tranferrin (5 µg ml^{-1}) (or ITS,1×, Sigma-Aldrich, I3146) + cholera toxin (0.1 µg ml^{-1}, Sigma-Aldrich, C9903) + EGF (25 ng ml^{-1}) + bovine pituitary extract (30 µg ml^{-1}, Sigma-Aldrich, P1476) + FBS (5%) + retinoic acid (0.05 µM). During the first 48 h of seeding or passage, 1 µM Y-27632 (MedChemExpress, HY-10583) was added to the base media. Media was changed every 2 d, and cells were passaged after ~1 week and every ~3–4 d for subsequent passages. Organoids were transduced as previously described.

Tumor implantation

Tumor organoids isolated from CAGs-rtTA3^{hom} / iBE^{hom} mice (engineered to contain four oncogenic SNVs) were engrafted into the flanks (subcutaneous injection) or livers (intrasplenic injection) of recipient mice. Subcutaneous tumors were allowed to grow for 10 d after injection, and mice were treated with dox (200 mg kg^{-1} in chow) for 1 week to induce BE expression. Flank tumors were imaged by IVIS (PerkinElmer) using the appropriate filters to visualize GFP and mScarlet. Liver tumors were allowed to grow for 6–8 weeks after implantation, and mice were treated with dox (200 mg kg^{-1} in chow) for 1 week before analysis.

Tumor digestion

After isolation, tumors were digested with Collagenase IV (2,000 U ml^{-1}) and DNAse (10,000 U ml^{-1}) in HBSS for 20 min at 37 °C in a shaking water bath. Then, cell suspensions were filtered through 40-µm cell strainers, washed and resuspended in EDTA-containing PBS supplemented with 3% FBS after erythrocyte lysis by osmotic shock.

Spleen and bone marrow cell suspensions

For the preparation of a single-cell suspension from bone marrow, femora and tibiae were removed and placed into cold PBS. Collection of bone marrow cells was performed by flushing the shaft with 5 ml using a 10-ml syringe with a 16-gauge needle. For the preparation of single-cell suspension from the spleen, the spleen was crushed and filtered through 40-µm cell strainers. Both cell suspensions were washed and resuspended in EDTA-containing PBS supplemented with 3% FBS after erythrocyte lysis by osmotic shock.

Generation of two-dimensional lines from organoids

To engineer immortalized two-dimensional lines, three-dimensional small intestinal organoids were transduced with a lentiviral all-in-one *Kras*^{G12D} cDNA and MultimiR tandem knockdown cassette (sh*Apc*-sh*Trp53*)[55]. After selection in media without RSPOI and Nutlin3 (10 µmol L^{-1}), organoids were split onto plates coated with Rat Collagen I in PBS (Gibco, A10483-01, 30 ng ml^{-1}) for 30 min at 37 °C before plating. Cells were passaged on collagen-coated plates 3–5 times and then split to plates without collagen. Two-dimensional cells were transduced with lentivirus as previously described[28].

Flow cytometry

Cells were trypsinized and organoids were mechanically dissociated, followed by TrypLE treatment at the indicated timepoint. Analysis of immune cell populations of spleen and bone marrow was performed after blocking Fc receptors by incubating with an anti-CD16/32 antibody (BioLegend, 101320) at 4 °C for 15 min. The cells were subsequently stained with fluorophore-conjugated antibodies using CD4-PE (BD Biosciences, 100408), CD8 PE-Cy7 (BD Biosciences, 100710), CD19 PE-Cy7 (BD Biosciences, 115509), CD11b PE (BD Biosciences, 101207),

GR1 PE (BD Sciences, 108407), CD45-APC (BD Biosciences, 103112) for 20 min at 4 °C in FACS buffer (PBS/2% FBS/3 mM EDTA), followed by staining with DAPI. Flow cytometry assays were carried out on a 2018 Attune NxT Flow Cytometer (Thermo Fisher Scientific). At least 25,000 events from the single-cell population gating were recorded, and gates were set as shown (Supplementary Fig. 6). All experiments were performed in replicates from independent mouse lines as annotated.

Organoid nucleofection

Three days before nucleofection, organoids were split for one well in a 12-well plate per condition and cultured in full media (ENR, 50 ng ml^{-1} EGF, Invitrogen and 50 nmol LDN-0193189, Selleck Chemicals + RSPOI conditioned media). Two days before nucleofection, media was changed to EN (50 ng ml^{-1} EGF, Invitrogen and 50 nmol, LDN-0193189, Selleck Chemicals) + Y-27632 (10 µmol L^{-1}) + CHIR99021 (5 µmol L^{-1}) and with or without dox as noted (500 ng ml^{-1}). On the day of nucleofection, media was removed, and organoids were mechanically dissociated in cold PBS by pipetting (50×). Organoid suspension was pelleted by spinning at 1,200 r.p.m. for 4 min at 4 °C and resuspended in 100 µl of TrypLE (Invitrogen, 12604), followed by incubation in a bead bath at 37 °C for 5 min. Next, ~300 µl of cold PBS was added, followed by mechanical dissociation of organoids by pipetting (50×) and then washed with cold PBS. Per condition, nucleofection mix was prepared as follows: 16.4 µl of Primary P3 Buffer (Lonza kit, V4XP-3032), 3.6 Supplement 1 (Lonza kit, V4XP-3032) and 1 µg of plasmid DNA or 200 pmol of chemically stabilized synthetic RNA (Synthego). For multiplexing experiments, total gRNA concentrations were kept constant and divided evenly by number of gRNAs in that condition. Pelleted organoids were resuspended in 20 µl of nucleofection mix and transferred to an electroporation chamber (Lonza kit, V4XP-3032, 96-well format) for electroporation using Lonza X Unit Nucleofector under the [ES, mouse] protocol. Organoids were recovered in 70 µl of media and washed once. Pelleted organoids were plated in original volume of Matrigel (BD Biosciences, 354230) and cultured in EN + Y-27632 + CHIR ± dox media for 2 d and subsequently replaced with full media or selection conditions. Nucleofection of WT organoids followed the same protocol electroporating the synthetic sgRNAs and an optimized BE (FNLS) cDNA (Addgene, 112671).

Organoid functional selection

To select for WNT-activating mutations, exogenous RSPOI was removed from the media. To select for loss-of-function *Trp53* mutations, Nutlin3 (5 µmol L^{-1}) was added to the media, and organoids were cultured for 10 d. To select for *Smad4* alterations, recombinant TGFB1 (5 ng ml^{-1}) was added to the media, and organoids were cultured for 7 d. To select for *Pik3ca*-activating mutations, selumetinib (1 µg ml^{-1}) was added to the media, and organoids were cultured for 14 d. Organoids were split as usual throughout selection conditions.

gDNA isolation

Cells and organoids were dissociated and pelleted at the indicated timepoint. Cells were lysed as previously described[8]. Tumor nodules were micro-dissected and homogenized using a 5-mm stainless steel bead (Qiagen, 69989) and a TissueLyser II (Qiagen) in 150 µl of gDNA lysis buffer for 3 min at a frequency of 30 Hz s^{-1} and immediately cooled for 5 min on ice. Tumor suspension was then lysed, and gDNA was isolated identical to cells[8].

PCR amplification for sequencing

Target genomic regions of interest were amplified by PCR using primers in Supplementary Table 2. PCR was performed with Herculase II Fusion DNA Polymerase (Agilent Technologies, 600675) according to the manufacturer's instructions using 200 ng of gDNA as a template and under the following PCR conditions: 95 °C × 5 min, 95 °C for 30 s → 57 °C for 30 s → 72 °C for 20 s × 39 cycles, 72 °C × 5 min. PCR products were confirmed using Qiaxel and purified using QIAquick PCR Purification Kit (Qiagen, 28106). PCR products were quantified by NanoDrop (Thermo Fisher Scientific) and normalized to 20 ng µl^{-1} in EB buffer. Targeted amplicon library preparation and next-generation sequencing (MiSeq, 2 × 250 bp) were performed at Azenta (previously GENEWIZ) and analyzed using CRISPResso2. Raw MiSeq FASTQ files have been deposited in the Sequence Read Archive (SRA) under accession number PRJNA859154.

Protein analysis

Organoids. A six-well of organoids was collected in Cell Recovery Solution (Corning, 354253) and incubated on ice for 30 min to 2 h and then washed with PBS three times to remove residual Matrigel. Organoid pellets were resuspended in 100 µl of RIPA buffer and centrifuged at 500*g* at 4 °C to collect protein supernatant.

Tissue. A 2-mg piece of each tissue was collected at indicated timepoints and immediately processed or snap frozen and stored at −80 °C. Tissue was homogenized in 150 µl of RIPA buffer with protease and phosphatase inhibitors by bead homogenizer (TissueLyser II, Qiagen) for 3 min at a frequency of 30 Hz s^{-1} and immediately cooled for 5 min on ice. The following antibodies were used for western blotting analysis of organoids and tissues: Cas9 (BioLegend, 844301) (1:500, 4 °C overnight) and actin (Abcam, ab49900) (1:10,000, 30 min at room temperature).

RNA isolation and RNA-seq

A six-well of organoids was collected in 800 µl of TRIzol (Invitrogen, 15596-026). The livers were removed and immediately homogenized for 15–20 s in 4 ml of TRIzol using a handheld homogenizer (Omni International, TM12500643). The intestinal villi were isolated by scrapping using glass slides and resuspended in 3 ml of TRIzol. Samples were immediately processed or stored at −80 °C. RNA was extracted according to the manufacturer's instructions. DNA contamination was removed through treatment with recombinant DNaseI (Roche Diagnostics, 04716728001) for 15 min at room temperature and column purification using Qiagen RNeasy Mini Kit (74106). cDNA was prepared from 1 µg of RNA (quantified by NanoDrop, Thermo Fisher Scientific). Weill Cornell Medicine's Genomics Core Laboratory checked RNA quality using a 2100 Bioanlyzer (Agilent Technologies), prepared the RNA library (TruSeq Stranded mRNA Sample Library Preparation Kit (Illumina)) and performed RNA-seq (single-end 75 cycles on a Illumina NextSeq 500). Raw FASTQ files have been deposited in the SRA under accession number PRJNA859154.

RNA-seq analysis

Raw FASTQ files were mapped to mouse (GRCm39) or human (GRCh38) reference genomes using STAR (version 2.4.1d, default parameters)[56]. STAR count data were used for estimating differential gene expression using DESeq2 (ref. 57). For data visualization and gene ranking, log fold changes were adjusted using lfcShrink in DESeq2. R (version 3.6.1) and R Studio (version 1.2.1335) were used to create all visualizations and principal component analysis. Volcano plots, heat maps and other visualizations were produced using the following software packages:

Enhanced Volcano (https://bioconductor.org/packages/devel/bioc/html/EnhancedVolcano.html)

pheatmap (https://www.rdocumentation.org/packages/pheatmap/versions/1.0.12/topics/pheatmap)

ggplot2 (https://cran.r-project.org/web/packages/ggplot2/index.html)

Variant calling was performed using picard (https://broadinstitute.github.io/picard/) and GATK (https://gatk.broadinstitute.org/hc/en-us) tools. Annotated single-nucleotide polymorphisms (SNPs) in the mouse (or human) *dbsnp* (https://ftp.ncbi.nlm.nih.gov/snp/) and Sanger Mouse Genomes Project (https://www.sanger.ac.uk/data/mouse-genomes-project/) were filtered from variant calls before

further analysis. The computational pipeline for picard and GATK, and code for processing variant tables and plotting, are available at https://github.com/lukedow/iBE.git.

Immunohistochemistry and immunofluorescence

Tissue was fixed, processed and imaged as previously described[54]. IDEXX RADIL performed hematoxylin and eosin (H&E) staining on paraffin-embedded sections. For immunofluorescence, primary antibodies used were rabbit anti-Cas9 (CST, 19526), mouse anti-p53 (CST, 2524), mouse anti-GS (BD Transduction Labs, 610517), mouse anti-β-catenin (CST, 2698), rabbit anti-CK19 (Abcam, ab133496), rabbit anti-α-SMA (Abcam, ab5694), rabbit anti-RFP (Rockland, AB_2209751), chicken anti-GFP (Abcam, ab13970) and rabbit anti-P-AKT (CST, 4060). Secondary antibodies used were donkey anti-rabbit 594 (1:500, Invitrogen, A21207) and donkey anti-mouse 647 (Invitrogen, A31571). All immunofluorescence sections were counterstained with DAPI.

HTVI

Next, 1 µg of SB13 transposase, 5 µg of SB-*Myc* and gRNA (20 µg of plasmid gRNA or 2 nmol Synthego synthetic standard chemically modified or 2 nmol Synthego synthetic heavily modified gRNA[58]) in 2 ml of saline were delivered by lateral teil vein injection over 5–7 s in 8–12-week-old mice. Tumors were harvested after palpation and at a humane endpoint.

Pancreas electroporation

Surgery to perform in vivo electroporation was previously described[59,60]. In brief, the surgical site is scrubbed with a povidone-iodine scrub (for example, Betadine and Nolvasan), and the site is then rinsed with 70% alcohol. Under isofluorane (2–3%) anesthetization, a small laparotomy is performed, and the pancreas is luxated with a blunt forceps. Then, 5 µg of SB13 transposase, 25 µg of SB-*Kras*^{G12D} and gRNA (20 µg of gRNA plasmid or 2 nmol Synthego synthetic heavily modified gRNA[58]) in 30-µl total volume (saline used to normalize) were delivered by injection into the pancreas. Solution is injected using a 27.5-gauge needle, and tweezer electrodes are tightly placed around the injection bubble. Two pulses of electrical current using an in vivo electroporator (NEPAGENE NEPA21 Type II in vitro and in vivo electroporator) are applied. After electroporation, the peritoneum cavity is rinsed with 0.5 ml of pre-warmed saline. Subsequently, the peritoneum and muscles are sutured with absorbable sutures, and the skin is closed with skin staples. The mice are kept at 37 °C until they are awake, and post-surgery pain management is done with injections of buprenorphine for the three following days (twice daily). Surgery and electroporation were performed on 8–12-week-old mice. Tumors were harvested after palpation and at a humane endpoint.

Statistical analysis

All statistical tests used are indicated in the corresponding figure legends. In general, to compare two conditions, a standard two-tailed unpaired *t* test was used, assuming variance between samples. In most cases, analyses were performed with one-way or two-way ANOVA with Tukey's correction for multiple comparisons. Unless otherwise stated, each replicate represents an independent mouse/organoid lines or tumors from $n \geq 3$ mice. Experimenters were not blinded to conditions. All statistics are reported in Supplementary Table 5.

Reporting summary

Further information on research design is available in the Nature Portfolio Reporting Summary linked to this article.

Data availability

All source data (including *P* values) are available in Supplementary Table 5. Raw FASTQ files have been deposited in the Sequence Read Archive under accession number PRJNA859154. Processed RNA-seq data (transcripts per million values and differentially expressed genes) are available in Supplementary Table 2.

Code availability

Code for analysis and data visualization is available at https://github.com/lukedow/iBE.git.

References

51. Dow, L. E. et al. A pipeline for the generation of shRNA transgenic mice. *Nat. Protoc.* **7**, 374–393 (2012).
52. O'Rourke, K. P., Ackerman, S., Dow, L. E. & Lowe, S. W. Isolation, culture, and maintenance of mouse intestinal stem cells. *Bio Protoc.* **6**, e1733 (2016).
53. Huch, M. et al. Unlimited in vitro expansion of adult bi-potent pancreas progenitors through the Lgr5/R-spondin axis. *EMBO J.* **32**, 2708–2721 (2013).
54. Zafra, M. P. et al. An in vivo *Kras* allelic series reveals distinct phenotypes of common ocogenic variants. *Cancer Discov.* **10**, 1654–1671 (2020).
55. Amen, A. M. et al. Endogenous spacing enables co-processing of microRNAs and efficient combinatorial RNAi. *Cell Rep. Methods* **2**, 100239 (2022).
56. Dobin, A. et al. STAR: ultrafast universal RNA-seq aligner. *Bioinformatics* **29**, 15–21 (2013).
57. Love, M. I., Huber, W. & Anders, S. Moderated estimation of fold change and dispersion for RNA-seq data with DESeq2. *Genome Biol.* **15**, 550 (2014).
58. Finn, J. D. et al. A single administration of CRISPR/Cas9 lipid nanoparticles achieves robust and persistent in vivo genome editing. *Cell Rep.* **22**, 2227–2235 (2018).
59. Paffenholz Stella, V. et al. Senescence induction dictates response to chemo- and immunotherapy in preclinical models of ovarian cancer. *Proc. Natl Acad. Sci. USA* **119**, e2117754119 (2022).
60. Leibold, J. et al. Somatic tissue engineering in mouse models reveals an actionable role for WNT pathway alterations in prostate cancer metastasis. *Cancer Discov.* **10**, 1038–1057 (2020).

Acknowledgements

We thank members of the Dow laboratory for advice and comments on the preparation of the paper. We would like to acknowledge K. Tsanov and J. Leibold for assistance and advice in setting up the pancreas EPO protocol. The content is solely the responsibility of the authors and does not necessarily represent the official views of the National Institutes of Health (NIH). This work was supported by a project grant from the NIH (R01CA229773), P01 CA087497 (S.W.L.), an MSKCC Functional Genomics Initiative grant (S.W.L.), an Agilent Technologies Thought Leader Award (S.W.L.) and support from Synthego under a Synthego Innovator Award (L.E.D.). A.K. was supported by an F31 Ruth L. Kirschstein Predoctoral Individual National Research Service Award (F31-CA247351-02). A.V. was supported by a Postdoctoral Fellowship from the Human Frontier Scientific Program (LT0011/2023-L). B.J.D. was supported by an F31 Ruth L. Kirschstein Predoctoral Individual National Research Service Award (F31-CA261061-01). E.E.G. is the Kenneth G. and Elaine A. Langone Fellow of the Damon Runyon Cancer Research Foundation (DRG-2343-18). F.J.S.R. was supported by the MSKCC TROT program (5T32CA160001) and a GMTEC Postdoctoral Researcher Innovation Grant and is a Howard Hughes Medical Institute (HHMI) Hanna Gray Fellow. S.W.L. is an HHMI investigator.

Author contributions

A.K. and A.V.P. designed and performed experiments, analyzed data and wrote the paper. M.F., J.Z., M.P.Z., S.G., E.G., J.S., W.L, B.J.D., M.C.F., K.H. and F.J.S.R. performed experiments and/or analyzed data.

S.W.L. supervised experimental work. L.E.D. designed and supervised experiments, analyzed data and wrote the paper.

Competing interests

L.E.D. is a scientific advisor and holds equity in Mirimus, Inc. L.E.D. has received consulting fees and/or honoraria from Volastra Therapeutics, Revolution Medicines, Repare Therapeutics, Fog Pharma and Frazier Healthcare Partners. S.W.L is an advisor for and has equity in the following biotechnology companies: ORIC Pharmaceuticals, Faeth Therapeutics, Blueprint Medicines, Geras Bio, Mirimus, Inc., PMV Pharmaceuticals and Constellation Pharmaceuticals. S.W.L. acknowledges receiving funding and research support from Agilent Technologies for the purposes of massively parallel oligo synthesis. K.H., A.P.K. and J.A.W. are employees and shareholders of Synthego Corporation.

Additional information

Extended data is available for this paper at https://doi.org/10.1038/s41587-023-01900-x.

Supplementary information The online version contains supplementary material available at https://doi.org/10.1038/s41587-023-01900-x.

Correspondence and requests for materials should be addressed to Lukas E. Dow.

Peer review information *Nature Biotechnology* thanks the anonymous reviewers for their contribution to the peer review of this work.

https://doi.org/10.1038/s41587-023-01900-x

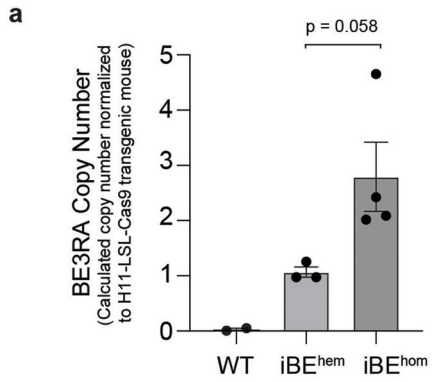

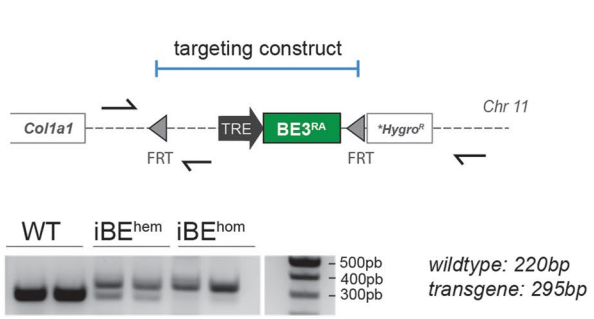

c

	iBE/-	rtTA3 / iBE/-
	Observed/Expected	Observed/Expected
Transmission	166/179	35/42.5
p-value	0.54	0.10

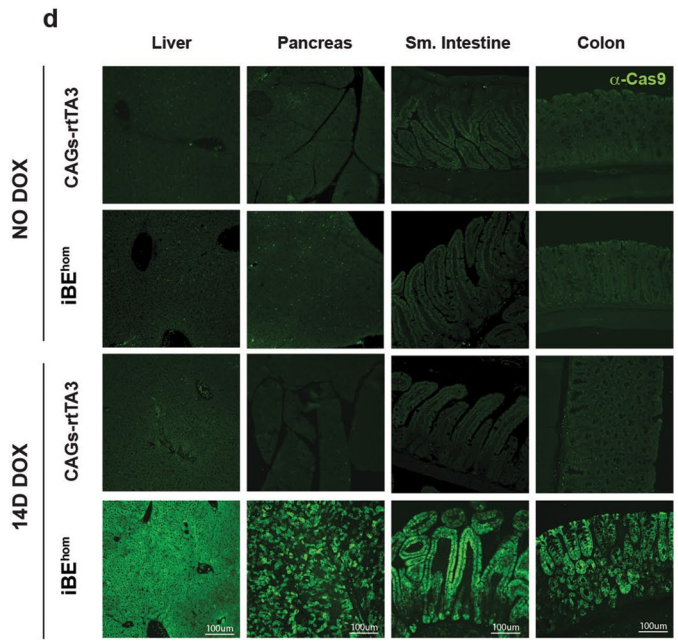

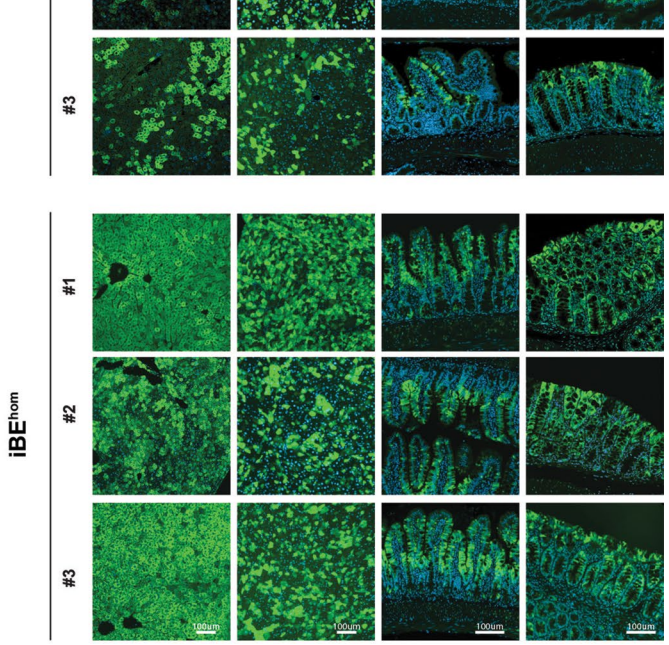

Extended Data Fig. 1 | Regulatable BE expression in vivo. a. Calculated BE3RA transgene copy number in iBE^{hem} and iBE^{hom} using a Taqman quantiative PCR assay with genomic DNA from H11-LSL-Cas9 mice as a reference. Data are presented as mean values ± s.e.m. (*p<0.05, Student's t-test). **b**. Schematic representation of the targeted RMCE site downstream of the Col1a1 locus. Primers flanking the knock-in cassette and a single primer within the targeted transgene can identify wildtype, hemizygous and homozygous animals, as shown in the example genotyping agarose gel **c**. Mendelian transmission of Col1a1-targeted iBE knock-in (with and without R26-CAGs-rtTA3 allele) and associated p-value (chi-square test) relative to expected Mendelian inheritance. **d**. Immunofluorescent detection of Cas9 protein in rtTA3 only and iBE^{hom} mice maintained on normal chow (No dox) or doxycycline chow for 14 days (14D dox). (n=3 mice per genotype and condition). **e**. Immunofluorescent detection of Cas9 protein in iBE^{hem} (top) or iBE^{hom} (bottom) mice maintained on dox chow for 7 days across four tissues. (n=3 mice per genotype and condition).

https://doi.org/10.1038/s41587-023-01900-x

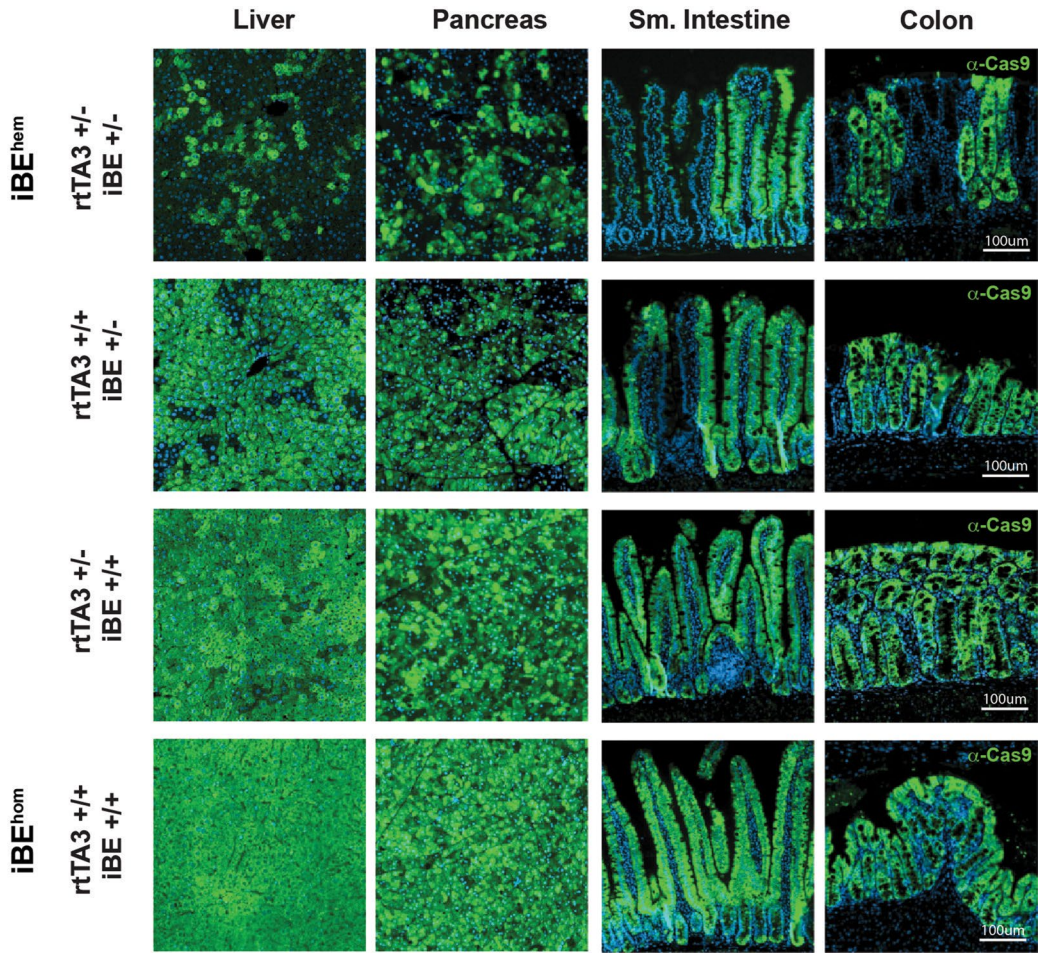

Extended Data Fig. 2 | Expression of BE3RA across different tissues in mice carrying one or two copy of each allele. Immunofluorescent detection of Cas9 protein in rtTA3$^{+/-}$ iBE$^{+/-}$ (iBE^{hem}), rtTA3$^{+/+}$ iBE$^{+/-}$, rtTA3$^{+/-}$ iBE$^{+/+}$ and rtTA3$^{+/+}$iBE$^{+/+}$ (iBE^{hom}) mice maintained on dox chow for 14 days. Cas9 protein(green), DAPI staining for nuclei (blue) across four tissues analyzed. (n=3 mice per genotype and condition).

https://doi.org/10.1038/s41587-023-01900-x

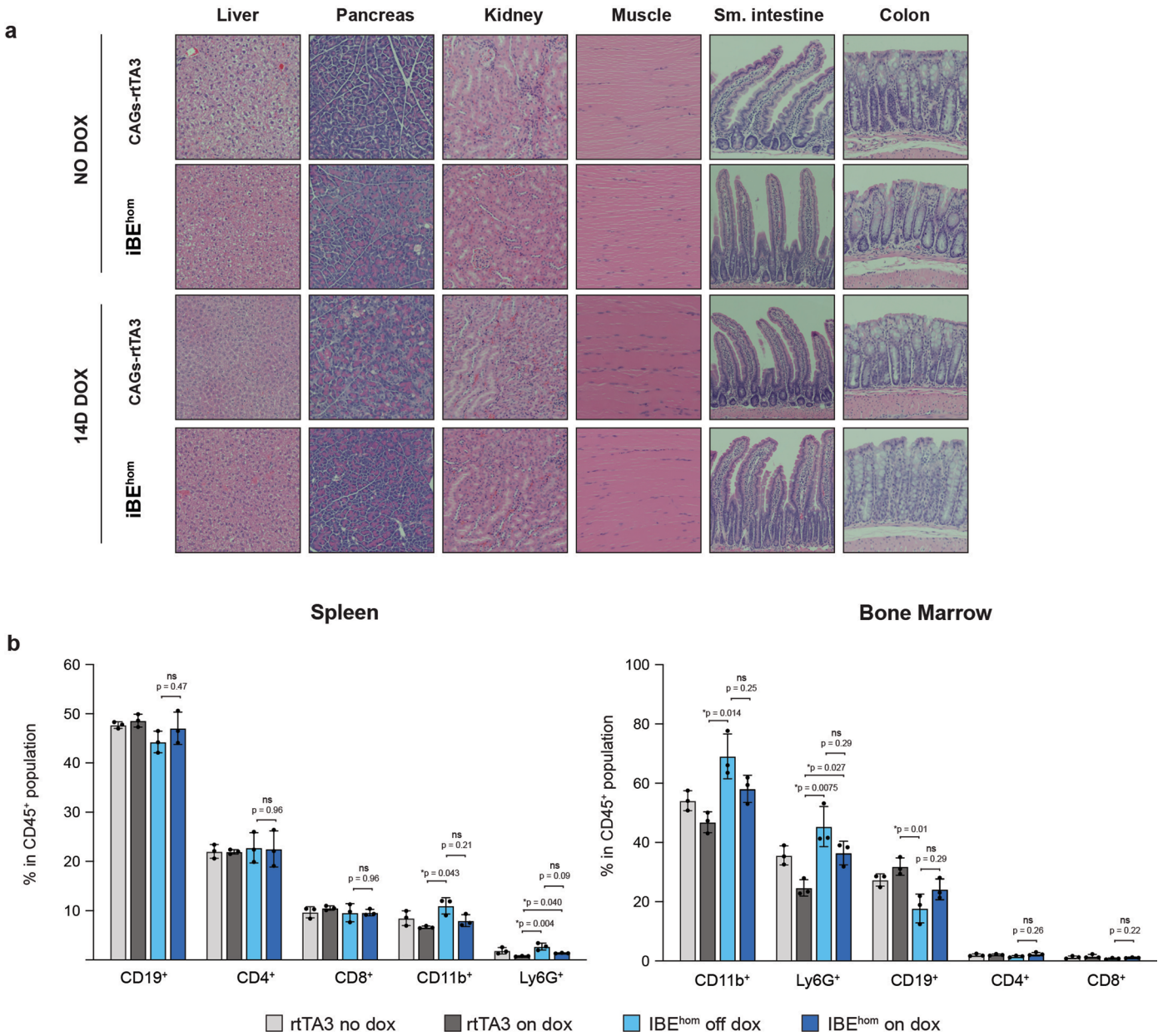

Extended Data Fig. 3 | Dox treatment does not induce abnormalities in iBEhom mice. a. Hematoxylin and Eosin (H&E) staining in rtTA3$^{+/-}$iBE$^{-/-}$ and rtTA3$^{+/+}$iBE$^{+/+}$ (iBE^{hom}) on normal chow or doxycycline chow for 14 days. (n=3 mice). **b**. Flow cytometry analysis of spleen and bone marrow cell suspensions of rtTA3$^{+/-}$iBE$^{-/-}$ and rtTA3$^{+/+}$iBE$^{+/+}$ (iBE^{hom}) on normal chow or maintained on doxycycline chow for 14 days (n=3 mice). Data are presented as mean values ± s.d (*p<0.05, Student's t-test).

https://doi.org/10.1038/s41587-023-01900-x

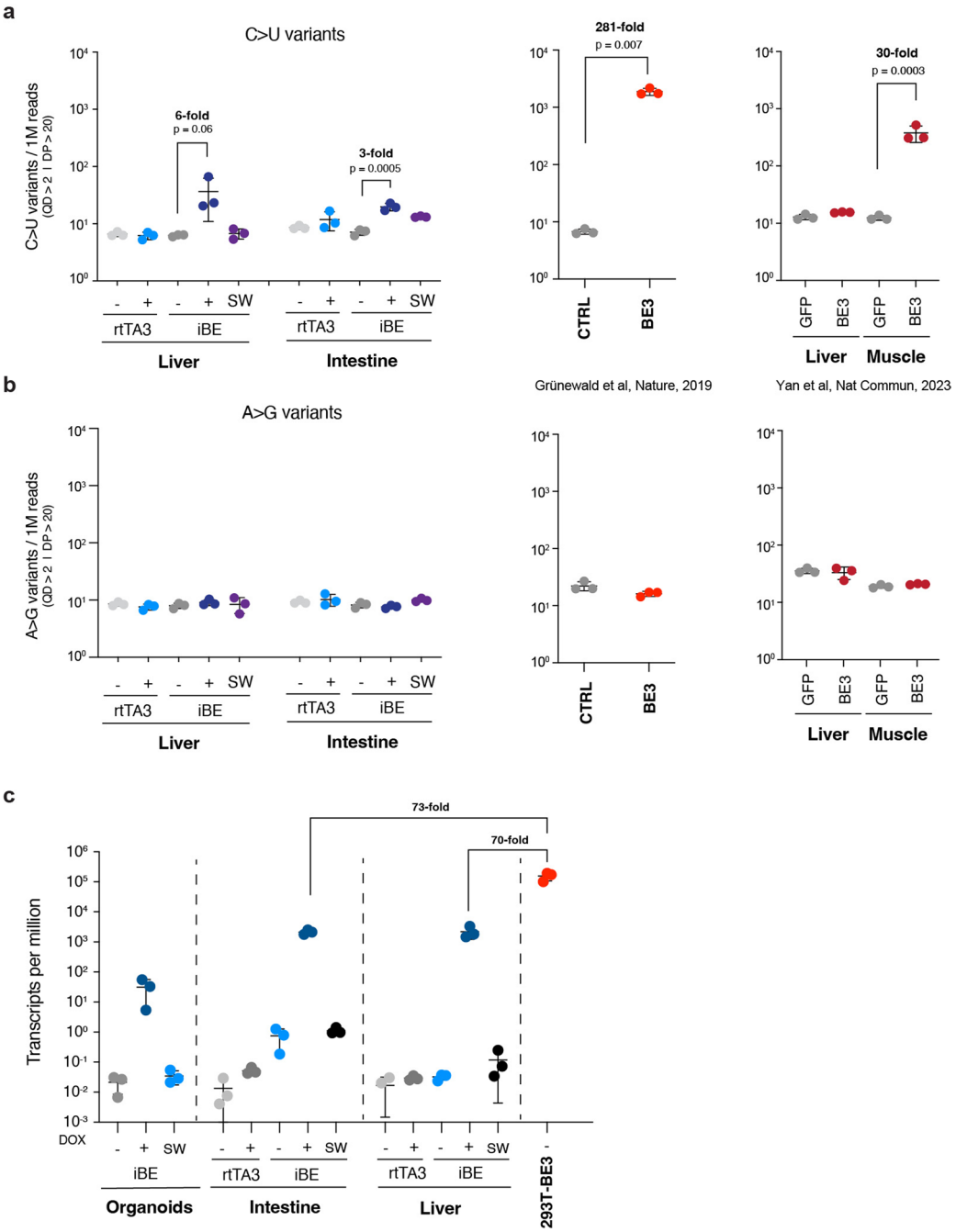

Extended Data Fig. 4 | iBE induces low off target RNA editing that is reversed by withdrawal of transgene expression. a. C to U editing in RNA transcripts detected from RNA sequencing data from intestine and liver from rtTA^{hem} and iBE^{hom} on normal chow (-), dox chow (+) for 14 days, or switched from dox chow for 14 days to normal chow for 6 days (SW). Data in the middle and right panels was derived from re-analysis of published datasets, as indicated under each plot. For experiments with multiple comparisons, p-values were calculated by one-way ANOVA, n=3 mice/condition. For individual pairwise comparisons, Student's t-test was used. **b**. A to G editing in RNA transcripts detected from RNA sequencing data from intestine and liver from rtTAhem and iBEhom on normal chow (-), dox chow (+) for 14 days, or switched from dox chow for 14 days to normal chow for 6 days (SW). (n=3 mice). **c**. Transcript abundance (transcripts per million; TPM) in pancreatic organoids, intestine, and liver from rtTA^{hem} and iBE^{hom} on normal chow (-), dox chow (+) for 14 days, or switched from dox chow for 14 days to normal chow for 6 days (SW). All data shown are presented as mean values +/- s.d., n=3 mice/condition.

https://doi.org/10.1038/s41587-023-01900-x

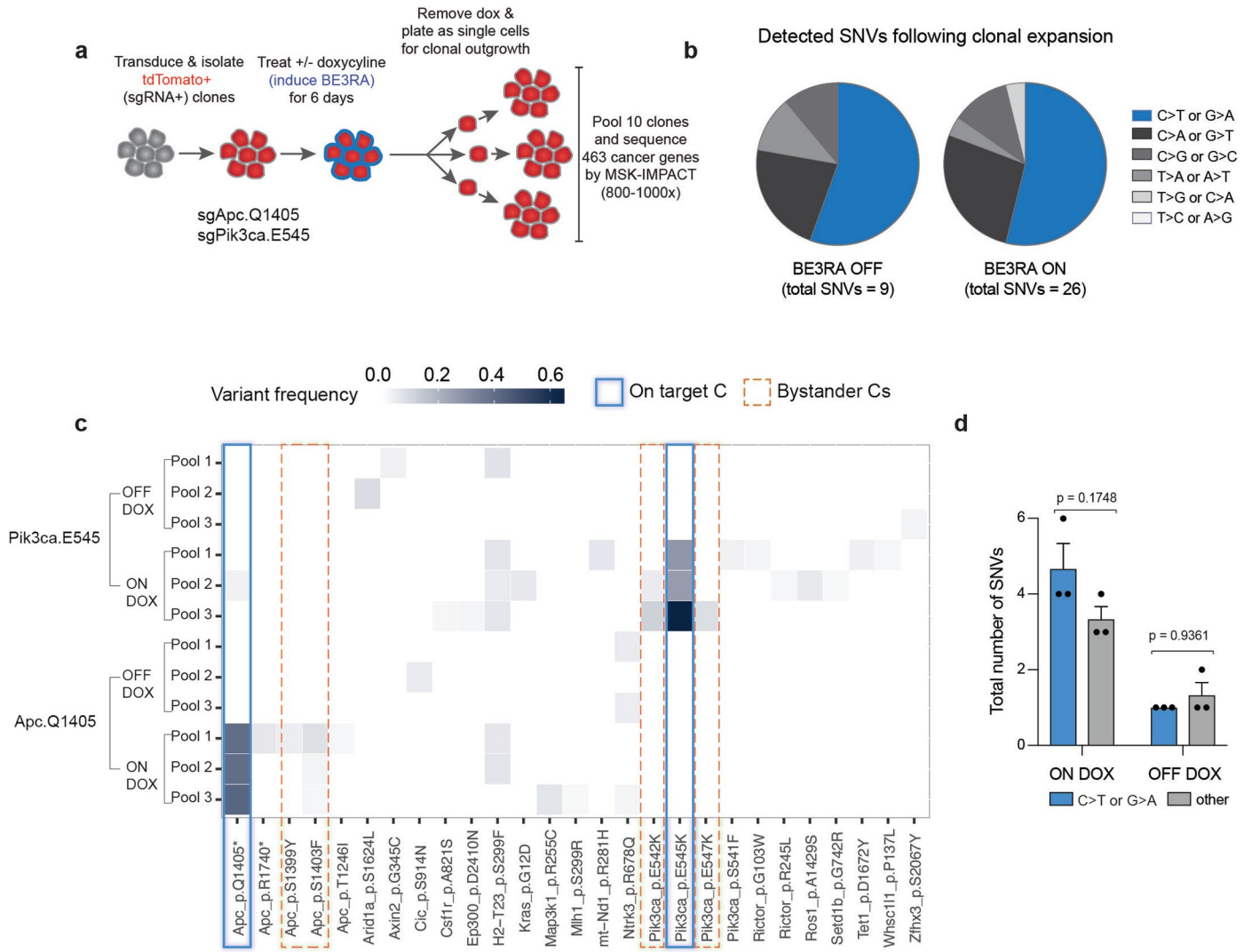

Extended Data Fig. 5 | iBE has low DNA off target activity. a. Schematic of experimental set up in mouse embryonic stem cells (ESCs). mESCs containing iBE knock in were transduced with LRT2B-gRNA vector and selected for gRNA expression. sgRNA+ cells were plated with and without dox for 6 days after which cells were plated at low density for clonal outgrowth without dox. 3 pools of 10 clones were picked for each dox conditions across to gRNA targeted cell lines (sgRNAs = Apc.Q1405X and Pik3ca.E545K). In total, 12 pools of 10 clones were sequenced at 800-1000-fold coverage across the MSK-IMPACT cancer gene set. **b.** Pie chart display of frequency of C>T or C>other SNVs found in pooled clones for each condition (on and off dox) for both sgRNAs. **c.** Sequencing analysis at cancer gene sites in cell conditions (right) described in a. Solid blue boxes represent on-target activity of the sgRNA, dotted orange boxes signify on-target 'bystander' editing within the gRNA window. **d.** Quantification of C>T and C>other SNVs found across both targets. 2-way ANOVA test for multiple comparisons was used to evaluate statistical significance across conditions. Data are presented as mean values ± s.e.m. p-values are displayed.

https://doi.org/10.1038/s41587-023-01900-x

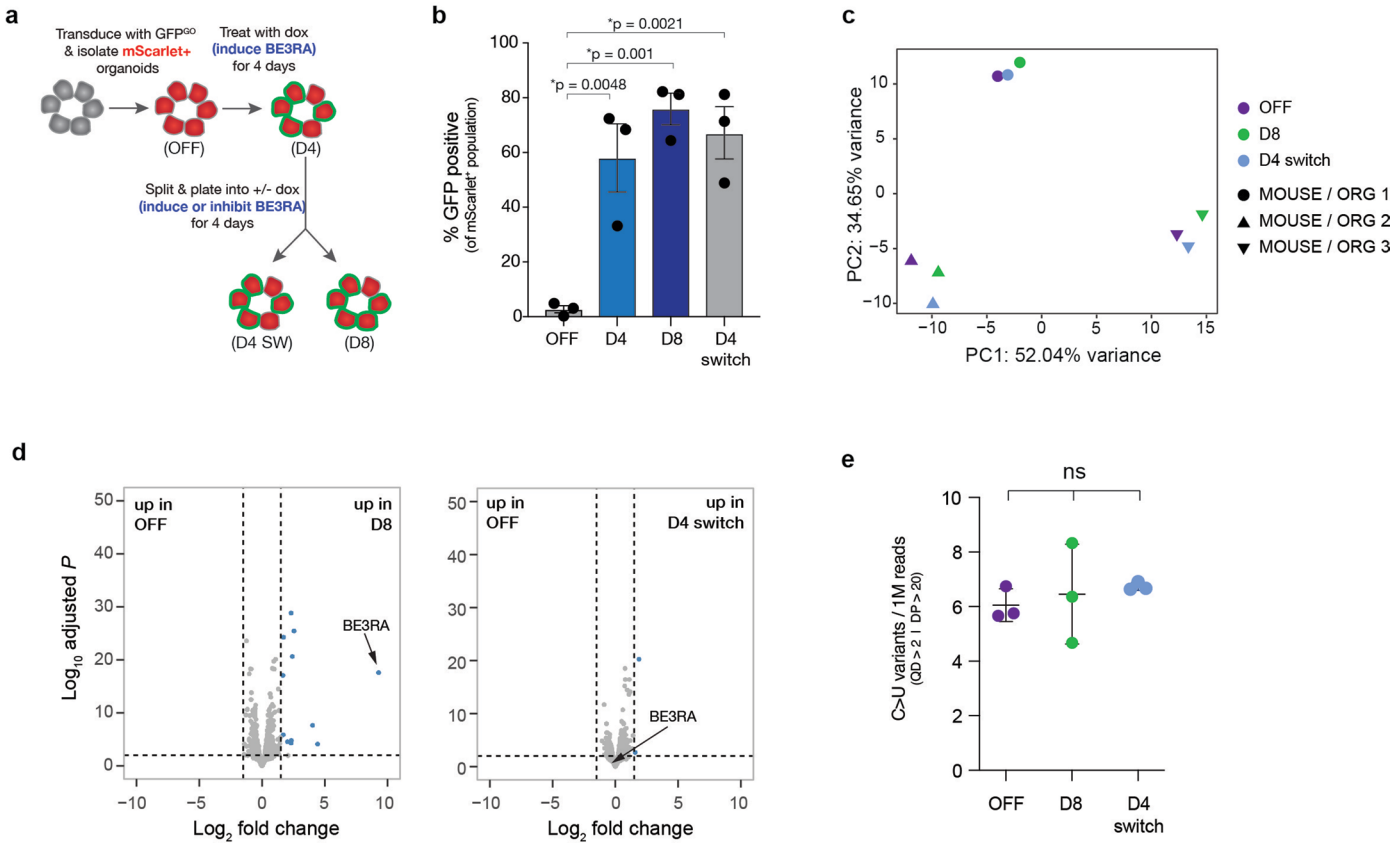

Extended Data Fig. 6 | iBE does not induce off target RNA editing in organoids. **a**. Schematic of experimental set up in iBE derived pancreatic organoids. Organoids were transduced and selected with GFP^{GO} reporter (mScarlet^{+}). Organoids maintained off dox were then split into dox conditions to induce BE expression for 4 days and then split again into + and − dox conditions for an additional day. **b**. Editing of organoids in each condition (OFF, D4, D8, and D4 sw) was quantified by flow cytometry, calculating the percentage of GFP^{+} cells within the mScarlet^{+} population. Data are presented as mean values ± s.e.m. One-way ANOVA with Tukey's correction **c**. PCA analysis of RNA sequencing data from OFF, D8, and D4 SW organoids. Colors correspond to dox condition and shape delineates organoid replicate/mouse origin (n=3). **d**. Volcano plots from RNA-seq data comparing iBE pancreatic organoids culture on dox-containing media vs regular media. **e**. Off-target RNA editing analysis, processed as described for Supplementary Fig. 4. No significant differences in RNA variants were observed, n=3, one-way ANOVA with Tukey's correction. Data are presented as mean values ± s.e.m. For all data shown, n=3 independent organoid lines/condition.

https://doi.org/10.1038/s41587-023-01900-x

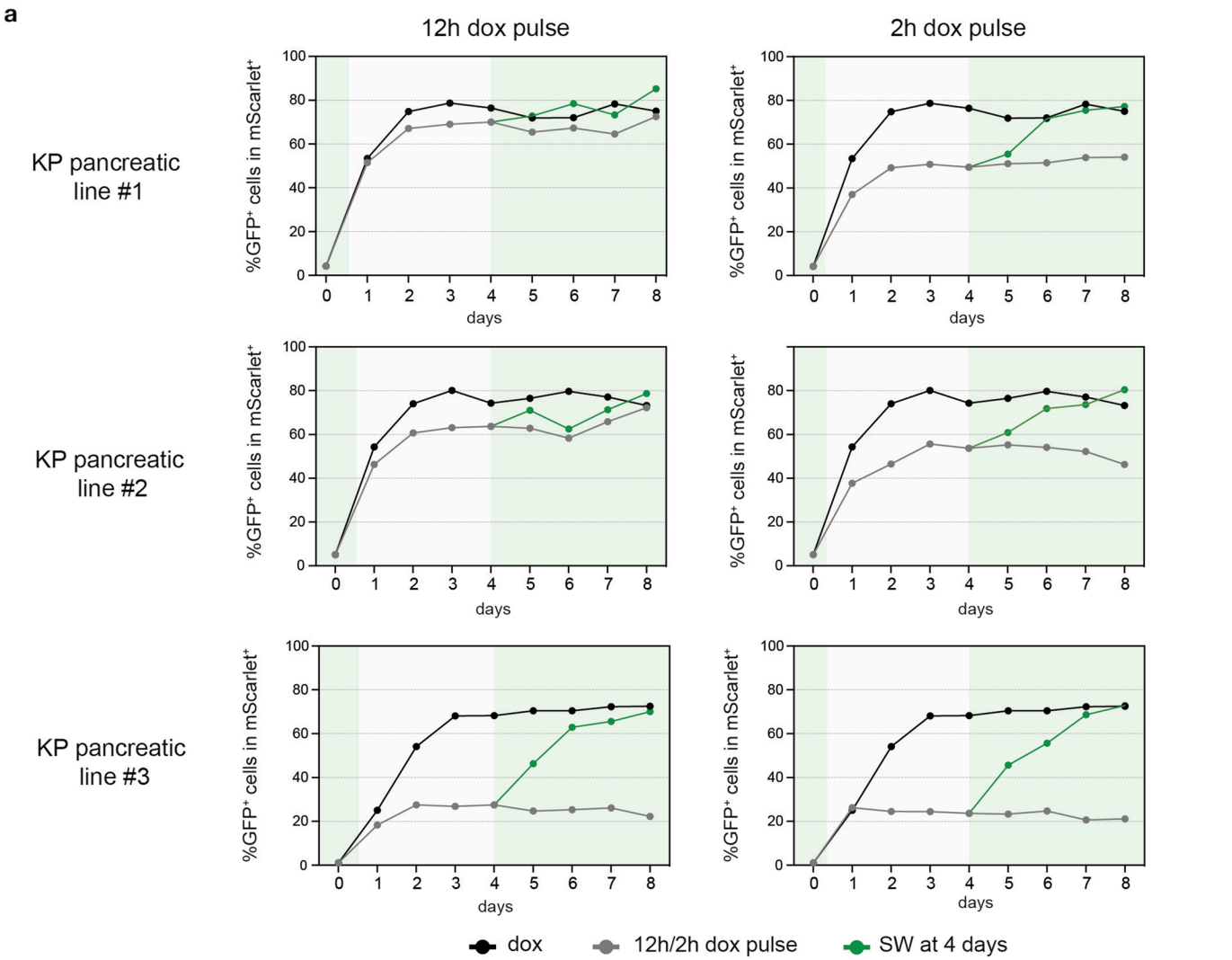

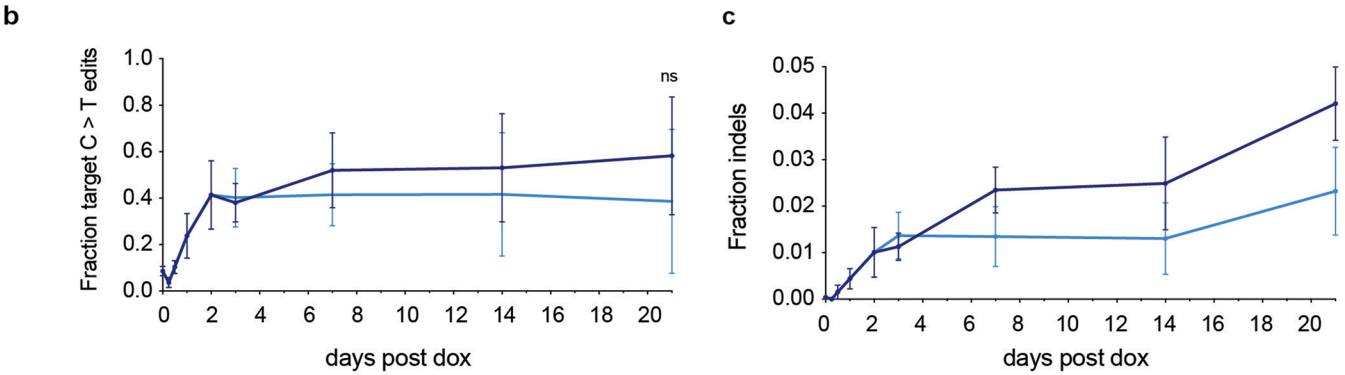

Extended Data Fig. 7 | Editing dynamics of iBE organoids. a. Flow cytometry analysis of three independent pancreatic KP mutant organoid lines integrated with GFP^{GO} reporter following dox treatment for 0-8 days (black), transient exposure for 2h or 12h (grey), or transient exposure then re-treatment at 4 days (green). **b.** Targeted deep sequencing quantification of target C:G to T:A conversion at the ApcQ1405X locus in 2D small intestinal derived iBE cell line following dox addition for 21 days (dark blue), or transient dox treatment for 3 days and withdrawn for 18 days (light blue). **c.** Targeted deep sequencing quantification of indel conversion of b. Data are presented as mean values ± s.e.m. (*p<0.05, Student's t-test) (n=3 independently derived line).

https://doi.org/10.1038/s41587-023-01900-x

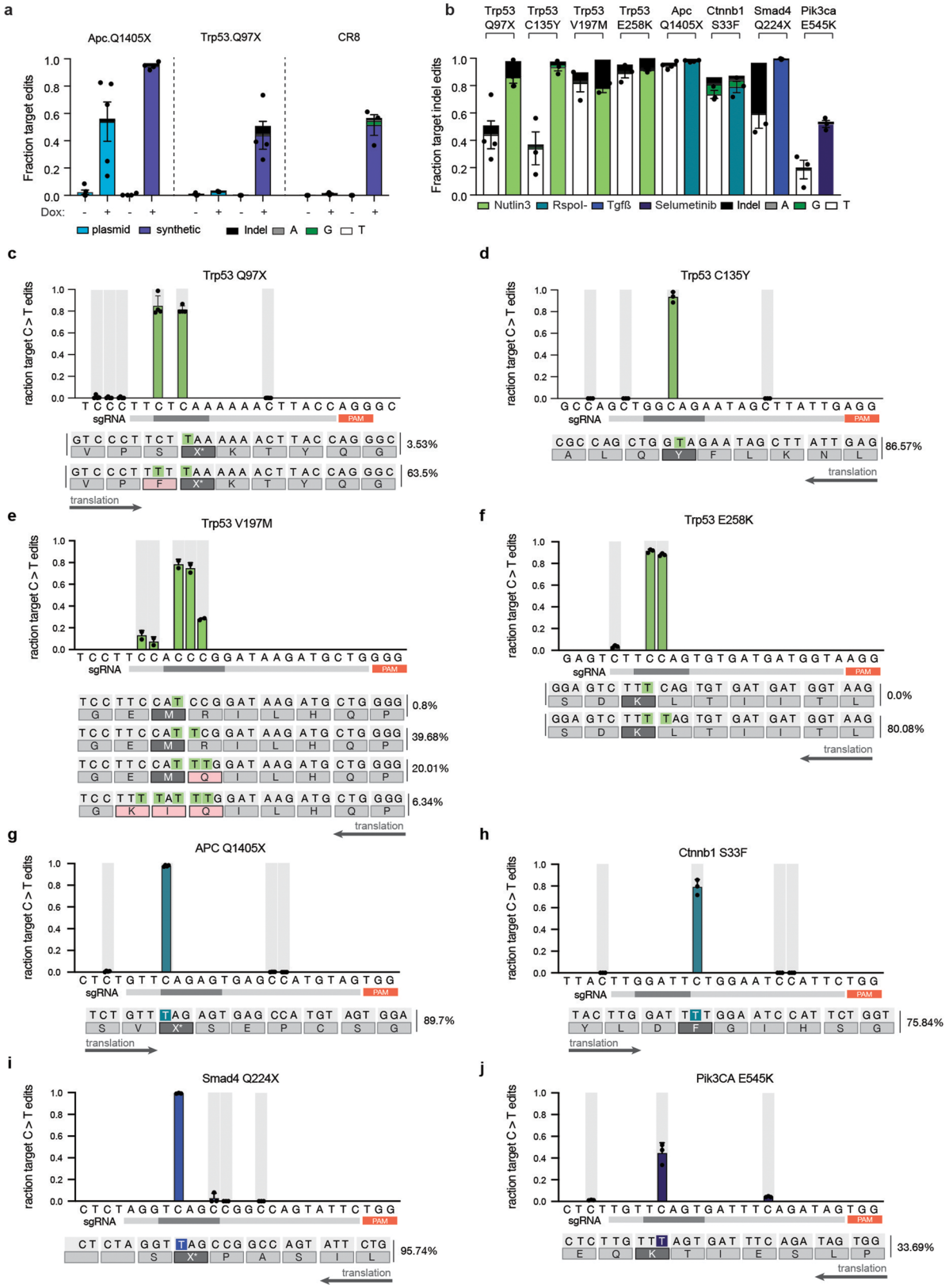

Extended Data Fig. 8 | Efficient BE in iBE organoids with low collateral editing. a. Targeted deep sequencing quantification of corresponding target C>T/A/G and indel conversion in small intestinal iBE organoids nucleofected with plasmid (light blue) or synthetic (indigo) gRNAs (ApcQ1405, Trp53Q97, CR8. OS2) as indicated, with and without dox treatment. **b**. Targeted deep sequencing quantification of target C>T/A/G and indel conversion in small intestinal iBE organoids nucleofected with synthetic gRNAs targeting cancer associated SNVs from Fig. 2f. **c-j**. Quantification of collateral editing of adjacent cytosines for samples shown in Fig. 2f. Predicted translation of each quantified read is shown below with targeted amino acid substitution (dark grey) and additional amino acid substitution (pink). All data are presented as mean values ± s.e.m.

https://doi.org/10.1038/s41587-023-01900-x

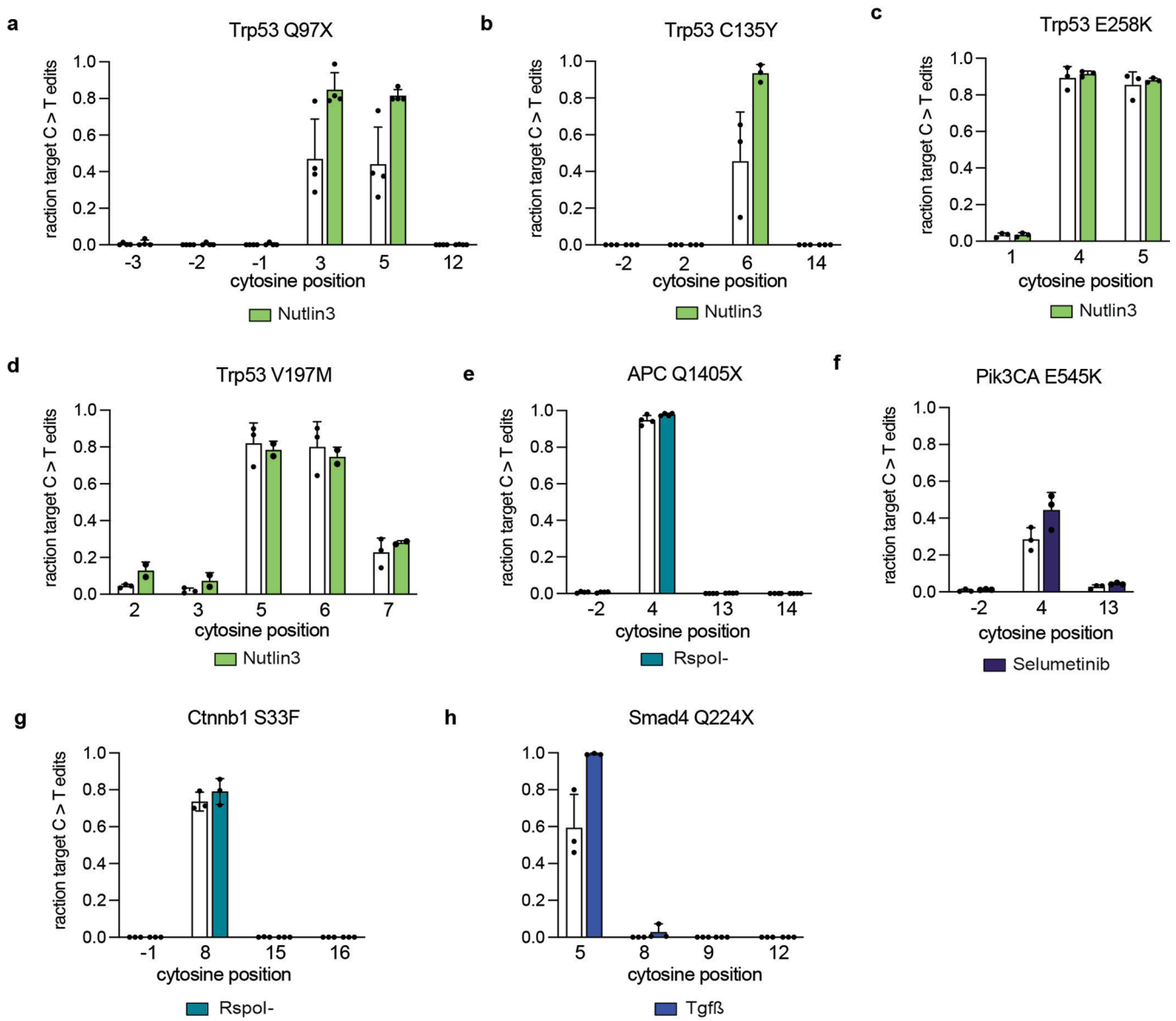

Extended Data Fig. 9 | Analysis of collateral editing before and after functional selection. a-h. Quantification of collateral editing of adjacent cytosines for data shown in Fig. 2f, unselected (white) and selected (color) in small intestinal iBE organoids nucleofected with various synthetic gRNAs targeting cancer associated SNVs.

https://doi.org/10.1038/s41587-023-01900-x

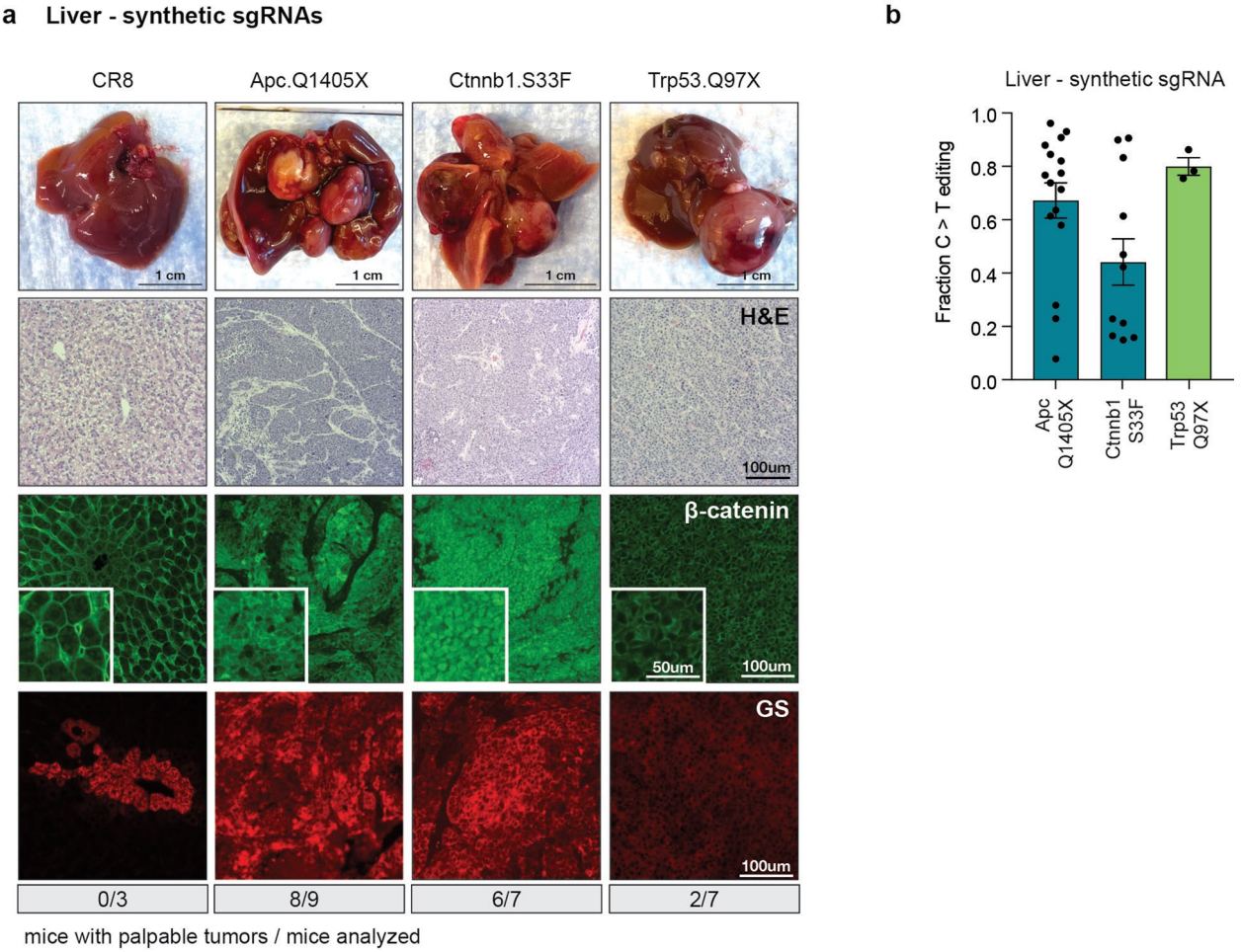

Extended Data Fig. 10 | In situ base editing with iBE by synthetic gRNA delivery drives liver tumors. a. HTVI delivery of synthetic gRNAs with *SB-Myc* as in Fig. 4. BF, H&E images, and IF staining for ß-catenin (green) and glutamine synthetase (GS, red) in livers with tumors. Number of transfected mice with palpable tumors is shown below each column. **b**. Quantification of target C:G to T:A conversion from tumors described in a). Each point corresponds to an isolated bulk tumor. (n=2-7 mice for a given gRNA target). Individual editing data color-coded by animal in Supplementary Fig. 3. All data are presented as mean values ± s.e.m.

nature portfolio

Corresponding author(s): Lukas Dow

Last updated by author(s): Jul 6, 2023

Reporting Summary

Nature Portfolio wishes to improve the reproducibility of the work that we publish. This form provides structure for consistency and transparency in reporting. For further information on Nature Portfolio policies, see our Editorial Policies and the Editorial Policy Checklist.

Statistics

For all statistical analyses, confirm that the following items are present in the figure legend, table legend, main text, or Methods section.

n/a	Confirmed	
☐	☒	The exact sample size (*n*) for each experimental group/condition, given as a discrete number and unit of measurement
☐	☒	A statement on whether measurements were taken from distinct samples or whether the same sample was measured repeatedly
☐	☒	The statistical test(s) used AND whether they are one- or two-sided *Only common tests should be described solely by name; describe more complex techniques in the Methods section.*
☒	☐	A description of all covariates tested
☐	☒	A description of any assumptions or corrections, such as tests of normality and adjustment for multiple comparisons
☐	☒	A full description of the statistical parameters including central tendency (e.g. means) or other basic estimates (e.g. regression coefficient) AND variation (e.g. standard deviation) or associated estimates of uncertainty (e.g. confidence intervals)
☐	☒	For null hypothesis testing, the test statistic (e.g. *F*, *t*, *r*) with confidence intervals, effect sizes, degrees of freedom and *P* value noted *Give P values as exact values whenever suitable.*
☒	☐	For Bayesian analysis, information on the choice of priors and Markov chain Monte Carlo settings
☒	☐	For hierarchical and complex designs, identification of the appropriate level for tests and full reporting of outcomes
☐	☒	Estimates of effect sizes (e.g. Cohen's *d*, Pearson's *r*), indicating how they were calculated

Our web collection on statistics for biologists contains articles on many of the points above.

Software and code

Policy information about availability of computer code

Data collection	Attune NxT flow cytometer software version 3.1, Illumina MiSeq, Illumnia NextSeq 500, Illumina NovaSeq
Data analysis	Graphpad Prism 8, FlowJo software version10.8, Geneious Prime, Adobe Illustrator, R, R studio, CRISPREsso2. R packages: STAR, DEseq2 ggplot2. Custom Github script for RNAseq analysis found at: https://github.com/lukedow/iBE.git.

For manuscripts utilizing custom algorithms or software that are central to the research but not yet described in published literature, software must be made available to editors and reviewers. We strongly encourage code deposition in a community repository (e.g. GitHub). See the Nature Portfolio guidelines for submitting code & software for further information.

Data

Policy information about availability of data

All manuscripts must include a data availability statement. This statement should provide the following information, where applicable:

- Accession codes, unique identifiers, or web links for publicly available datasets
- A description of any restrictions on data availability
- For clinical datasets or third party data, please ensure that the statement adheres to our policy

Plasmids will be made available at Addgene. Raw sequencing data is available at the sequence read archive (SRA) under accession: PRJNA859154

Field-specific reporting

Please select the one below that is the best fit for your research. If you are not sure, read the appropriate sections before making your selection.

☒ Life sciences ☐ Behavioural & social sciences ☐ Ecological, evolutionary & environmental sciences

For a reference copy of the document with all sections, see nature.com/documents/nr-reporting-summary-flat.pdf

Life sciences study design

All studies must disclose on these points even when the disclosure is negative.

Sample size	For experiments involving animals, 5-15 mice were used per sgRNA. This number allows detection of 50% difference between samples, with 80% power (assuming 20% variance).
Data exclusions	*Describe any data exclusions. If no data were excluded from the analyses, state so OR if data were excluded, describe the exclusions and the rationale behind them, indicating whether exclusion criteria were pre-established.*
Replication	Ex vivo manipulations were performed in 3 biological replicates (where each organoid lines is derived from a different mouse). In vivo manipulations were performed in 5-15 mice to allow for power and minimum of n=3 tumor derived mice for study.
Randomization	No samples were randomized
Blinding	Researchers were not blinded to experiments or analyses

Reporting for specific materials, systems and methods

We require information from authors about some types of materials, experimental systems and methods used in many studies. Here, indicate whether each material, system or method listed is relevant to your study. If you are not sure if a list item applies to your research, read the appropriate section before selecting a response.

Materials & experimental systems

n/a	Involved in the study
☐	☒ Antibodies
☐	☒ Eukaryotic cell lines
☒	☐ Palaeontology and archaeology
☐	☒ Animals and other organisms
☒	☐ Human research participants
☒	☐ Clinical data
☒	☐ Dual use research of concern

Methods

n/a	Involved in the study
☒	☐ ChIP-seq
☐	☒ Flow cytometry
☒	☐ MRI-based neuroimaging

Antibodies

Antibodies used	anti-CD16/32 antibody (Biolegend, #101320), CD4-PE (BD, #100408), CD8 PE-Cy7 (BD, #100710), CD19 PE-Cy7 (BD,115509), CD11b PE (BD, #101207), GR1 PE (BD, #108407), CD45-APC (BD, #103112), Cas9 (Biolegend, #844301), Actin (Abcam ab49900), anti-Cas9 (CST, #19526), mouse anti-p53 (CST, #2524), mouse anti-Glutamine synthetase (GS; BD Transduction Labs #610517), mouse anti-b-catenin (CST, #2698), rabbit anti-Cytokeratin-19 (CK19, Abcam, #ab133496), rabbit anti- alpha Smooth muscle actin (aSMA, Abcam, #ab5694), rabbit anti-RFP (Rockland, AB_2209751), chicken anti-GFP (Abcam, #ab13970), rabbit anti-P-AKT (CST, #4060), donkey anti-rabbit 594 (1:500, Invitrogen, #A21207), donkey anti-mouse 647 (Invitrogen, #A31571).
Validation	Antibodies were used as described by manufacturer's recommendation for murine tissue staining.

Eukaryotic cell lines

Policy information about cell lines

Cell line source(s)	Organoid lines were isolated and propagated from stem cell population of mouse tissues. HEK293T (ATCC CRL-3216) cells were purchased from the ATCC.
Authentication	Mice genotype was confirmed prior to organoid generation. Organoids were genotyped but not authenticated. HEK293Ts were purchased from ATCC and frozen at low passage.
Mycoplasma contamination	Organoids kept in culture were routinely tested for mycoplasma and discarded if tested positive

Commonly misidentified lines (See ICLAC register)	NA

Animals and other organisms

Policy information about studies involving animals; ARRIVE guidelines recommended for reporting animal research

Laboratory animals	Mice were maintained under specific pathogen-free conditions, and food and water were provided ad libitum. ES cell-derived mice were produced by injection into albino B6 blastocyst by the transgenic targeting core facility at NYU School of Medicine. High chimera (agouti) founders were transferred to Weill Cornell Medicine facilities and backcrossed to C57Bl/6 mice for at least 4 generations before analysis. All mice used for organoids were 6 to 8 week-old mix of males and females. All mice injected for in vivo tumor analysis were injected at 6 weeks and tumors harvested after 6-10 weeks and were a mix of males and females.
Wild animals	NA
Field-collected samples	NA
Ethics oversight	All animal experiments were approved by the Weill Cornell Medicine Institutional Animal Care and Use Committee (IACUC) under protocol 2014-0038 or by the MSKCC Institutional Animal Care and Use Committee under protocol 11-06-018.

Note that full information on the approval of the study protocol must also be provided in the manuscript.

Flow Cytometry

Plots

Confirm that:

☒ The axis labels state the marker and fluorochrome used (e.g. CD4-FITC).

☒ The axis scales are clearly visible. Include numbers along axes only for bottom left plot of group (a 'group' is an analysis of identical markers).

☒ All plots are contour plots with outliers or pseudocolor plots.

☒ A numerical value for number of cells or percentage (with statistics) is provided.

Methodology

Sample preparation	Organoids derived from mice were dissoicated into single cells, stained with DAPI and diluted for flow.
Instrument	Attune NxT flow cytometer
Software	Attune NxT flow cytometer software version 3.1 was used to collect. and FlowJo software version10.8
Cell population abundance	Ex vivo organoids are pure prior to dissociation. No selection necessary.
Gating strategy	All cells are gated by FSC-A/SSA around smaller sized population and then gated for single cells based on linear trajectory followed by gating on live cells (DAPI negative cells). Negative to positive boundaries were selected based on negative and single positive controls during voltage setting.

☒ Tick this box to confirm that a figure exemplifying the gating strategy is provided in the Supplementary Information.